G𝓛OO31𝟸

UNITED STATES DEPARTMENT OF THE INTERIOR

GEOLOGICAL SURVEY

Geology, geochronology, and potential volcanic hazards in the

Lava Ridge-Hells Half Acre area, eastern Snake River Plain, Idaho

by

Mel A. Kuntz

and

G. Brent Dalrymple

Open-File Report 79-1657

This report is preliminary and has not
been edited or reviewed for conformity
with U.S. Geological Survey standards.

Contents

Contents (cont.)

Illustrations

_____

Illustrations (cont.)

Tables

ABSTRACT

The evaluation of volcanic hazards for the proposed Safety Test Reactor Facility (STF) at the Argonne National Laboratory-West (ANLW) site, Idaho National Engineering Laboratory (INEL), Idaho, involves an analysis of the geology of the Lava Ridge-Hells Half Acre area and of K-Ar age determinations on lava flows in cored drill holes. The ANLW site at INEL lies in a shallow topographic depression bounded on the east and south by volcanic rift zones that are the locus of past shield-type basalt volcanism and by rhyolite domes erupted along the ring fracture of an inferred rhyolite caldera. The K-Ar age data indicate that the ANLW site has been flooded by basalt lava flows at irregular intervals from perhaps a few thousand years to as much as 300,000-400,000 years, with an average recurrence interval between flows of approximately 80,000-100,000 years. At least five major lava flows have covered the ANLW site within the past 500,000 years.

INTRODUCTION

This report summarizes the geology of the Lava Ridge-Hells Half Acre
area, a strip across the central part of the eastern Snake River Plain;
radiometric age studies of basalt lava flows sampled in drill cores; and the
implications for volcanic hazards at the facilities of the Argonne National
Laboratory-West (ANLW), Idaho National Engineering Laboratory (INEL). Cores
from five drill holes at the proposed STF reactor facility site at the ANLW
facilities were studied and logged, and individual lava flows were
identified. The STF reactor was formerly called the SAREF reactor. The
present "SAREF project" at ANLW includes the STF reactor and 3 other
projects. A correlation chart showing the lava-flow stratigraphy at the STF
site was prepared from these data (Kuntz, 1978a). The potassium-argon age
study on 15 rock samples from five lava flows identified in the drill cores
forms the basis of the evaluation of the recurrence interval of lava flows at
the ANLW facilities site.

The geology and volcanology of the Snake River Plain are described in
other reports (Armstrong and others, 1975; Kuntz, 1978b; LaPoint, 1977; Mabey,
1978; Malde and Powers, 1962; Christiansen and McKee, 1978); they are
discussed here briefly to provide a background for the interpretation of the
volcanic hazards for the ANLW facility. A geologic map of the Lava Ridge-
Hells Half Acre area of the eastern Snake River Plain (Kuntz and others, 1979)
contains field data and locates geographic features pertinent to this study.
The map is referred to frequently throughout this report.

The Snake River Plain is a topographic depression 50-100 km wide and
600 km long that cuts an arcuate trough across southern Idaho (fig. 1). It
extends from Payette on the west for about 300 km southeast to Twin Falls and
then for about 300 km northeast to Ashton, forming a continuous physiographic
feature.

Figure 1.--Generalized map of southern Idaho showing geographic and geologic

features referred to in the text. Major normal faults are generalized

and shown by heavy lines. The Lava Ridge-Hells Half Acre area is

outlined by short dashed lines.

Montana
45° N. Lat.

Beaverhead

Leadore

Centennial Range

Yellowstone Volcanic Plateau

Idaho Batholith

Lost River Range

Lemhi Range

Ashton

Juniper Buttes

St. Anthony

Payette

PIONEER Range

Arco

Big Hole

Teton R.

Western Snake River Plain

Big Southern Butte

Eastern Snake River Plain

Caribou Range

Portneuf Range

Bear River Range

Owyhee

Volcanic

Plateau

Twin Falls

Sublette Range

Deep Creek R.

Bannock Range

Oregon

Albion Range

Cotterel Range

Nevada

Utah

Wyoming

42° N. Lat.

117° W. Long.

119° W. Long.

111° W. Long.

0   50   100

KM

The plain is bounded on the north by Mesozoic to early Tertiary granitic rocks of the Idaho batholith and by folded Paleozoic and Mesozoic rocks in block-fault mountains that were uplifted along normal faults in Tertiary and Quaternary time during Basin and Range tectonism. The plain is bounded on the southeast by folded Paleozoic and Mesozoic rocks in fault-block mountains of the Basin and Range province that were also uplifted along normal faults in Tertiary and Quaternary time. Tertiary rhyolitic and basaltic volcanic rocks of the Owyhee Volcanic Plateau bound the plain on the southwest, and late Tertiary-Quaternary rhyolitic and basaltic volcanic rocks of the Yellowstone Volcanic Plateau occur at the northeast end of the plain (fig. 1).

Geologists divide the Snake River Plain into two parts, the western and eastern Snake River Plain (hereafter abbreviated WSRP and ESRP), at about 114° W. longitude. The two parts of the plain have different structural, geological, and geophysical characteristics. Because the area discussed in this report is located in the ESRP (fig. 1) a brief, general discussion of the geology of that region is given here.

The ESRP is a broad, flat lava plain consisting, at the surface, of basalt lava flows and interbedded, thin, discontinuous deposits of loess, eolian sand, and alluvial-fan materials. Drilling and geophysical studies (Zohdy and Stanley, 1973; Stanley and others, 1977) suggest that the lava flows and sediments have a total thickness of about 1-2 km near the Lava Ridge-Hells Half Acre area. Drainage is dominated by the Snake River which flows along the southeast margin of the ESRP. A topographic ridge of volcanic constructional origin extends from Big Southern Butte northeastward to Juniper Buttes near St. Anthony and coincides with the long axis of the ESRP (fig. 1). Rivers entering the ESRP from the mountains north of the plain are deflected by the ridge into closed basins.

Lava flows on the ESRP were erupted from low volcanic vents, most of which are alined along volcanic rift zones. The volcanic rift zones trend at right angles to the long axis of the ESRP, and many appear to be extensions of range-front faults which bound block-fault mountains on the margins of the ESRP (Kuntz, 1977a, 1977b, 1977c, 1978b). Magnetic polarity studies by Kuntz indicate that, with a few local exceptions, surface flows throughout the ESRP are of normal polarity. In addition, field evidence such as morphology of lava flows, degree of erosion, and stratigraphic relationships with surficial deposits indicate that the flows are young; thus they were erupted within the Brunhes magnetic polarity epoch which began about 700,000 years ago. Radiocarbon ages of organic soils which were buried beneath lava flows (Meyer Rubin and Elliott Spiker, U.S. Geological Survey, written commun., 1977, 1978, 1979; Valastro and others, 1972) show that volcanism has occurred throughout the ESRP in the last 15,000 yrs.

The origin and early volcanic history of the ESRP are not clearly known at present, because rocks which record that part of its history are largely buried by basalt lava flows and interbedded sediments. The problem is complicated by the fact that the regional drainage has not created deep canyons in which the older rocks would be exposed. Until several months prior to the time of this writing, few drill holes had penetrated deeper than the uppermost parts of the water table (average depth of about 100-300 m) beneath the surface of the ESRP. Four drill holes have been drilled to depths ranging from 610 to 3,158 m (2,000 to 10,360 ft) since 1978. Implications taken from the rock types encountered in those wells are still under investigation, but preliminary results suggest that rhyolitic ash flows and lava flows are present beneath the basalt-sediment cover of the eastern Snake River Plain in some localities (Doherty and others, 1979).

Available geological, geophysical, radiometric-age, and drilling data suggest that the ESRP has been the site of a northeasterly propagating, rhyolitic volcanic system which began in mid-Miocene time. Rhyolitic calderas began to form near Twin Falls about 14 m.y. ago and each successively younger caldera occurred farther to the northeast. The youngest caldera in the chain was formed about 600,000 years ago in Yellowstone National Park. Caldera formation is believed to be initiated and followed by the generation of tholeiitic basalt magma formed in the mantle by shear melting. Melting of the mantle and partial melting of the lower crust produces the bimodal basalt-rhyolite volcanism so characteristic of the ESRP, WSRP, and Great Basin during the last 17 m.y. Such a volcanic system produces high heat flow, thinning and decreased rigidity of the crust, and the progressive formation of a topographic trough along the chain of calderas. The location of the caldera chain in the ESRP was governed by a poorly understood and complex interaction in the late Tertiary between lithospheric plates of the Western United States and a Precambrian zone of structural weakness in the crust. Details of this model are provided by Eaton and others (1975), Christiansen and McKee (1978), and Mabey and others (1978).

GEOLOGY OF THE LAVA RIDGE-HELLS HALF ACRE AREA

Physiography and Drainage

The Lava Ridge-Hells Half Acre map area (Kuntz and others, 1979) covers a roughly rectangular region about 80 km long and 43 km wide in southeastern Idaho. It includes the southern tips of three mountain ranges and extends southeasterly to approximately 15 km southeast of the northeast-trending long axis of the ESRP (fig. 1). The three mountain ranges, Lost River, Lemhi, and Beaverhead, are long and narrow; they are about 20 km wide and are separated by intervening alluviated valleys, also about 20 km wide. Within the map

area, range crests reach elevations of as much as about 3,290 m (10,800 ft).
The average elevation of the intermontane valleys at their mouths along the
northwest margin of the ESRP is about 1,460 m (4,800 ft).

The topographic ridge of volcanic constructional origin, with an average
elevation of about 1,650 m (5,400 ft), coincides with the long axis of the
ESRP in the Lava Ridge-Hells Half Acre area (fig. 2). Thus the surface of the
ESRP slopes gently away from the ridge, toward the foot of the mountain ranges
and the mouths of the intermontane valleys at the northwest margin, and toward
the Snake River on the southeast margin of the ESRP.

The Little Lost River and Birch Creek drain the intermontane valleys in
the map area and end in closed basins, the Little Lost River sinks and the
Birch Creek sinks respectively, located along the northwest margin of the ESRP
(fig. 2). The natural course of these rivers is across the ESRP to the Snake
River, the major drainage in southern Idaho, but that course is blocked by the
topographic ridge. The Big Lost River enters the ESRP at Arco (fig. 1) and is
deflected to the northeast by the topographic ridge, where it ends in the Big
Lost River sinks (fig. 2). The Snake River and its tributaries extend along
the southeast margin and drain the intermontane valleys southeast of the ESRP.

Surficial Deposits

Surficial deposits in the Lava Ridge-Hells Half Acre area are largely
confined to the intermontane valleys, the lower slopes of the mountain ranges,
and the area of the closed basins, and along the Big Lost River. Mainstream
terrace deposits consisting of well-bedded gravel and sand and ranging in age
from early Pinedale to the present occur along Birch Creek and the Little Lost
and Big Lost Rivers. Alluvial fans consisting of crudely bedded gravel extend
from the range fronts to the mainstreams in the intermontane valleys. The

Figure 2.—Location map showing volcanic vents, open fissures, volcanic rift
   zones, ring fracture of an inferred caldera and rhyolite domes in the
   Lava Ridge-Hells Half Acre area. Abbreviations used: LLRS-Little Lost
   River sinks, BLRS-Big Lost River sinks, BCS-Birch Creek sinks,
   ANLW-Argonne National Laboratory-West facilities.

EXPLANATION

- Volcanic vent showing orientation of feeder fissure.
- Open fissures
- Volcanic rift zone
- Long axis of ESRP
- Rhyolite dome
- Ring fracture

Little Lost River

Lemhi Range

Howe fault

Berenice

Lost River Range

LLRS

Howe

BLRS

Birch Creek

BCS

State Highway 88

Circular Butte

43°45' N.

Circular Butte - Kettle Butte Volcanic Rift Zone

Lava Ridge - Hells Half Acre Volcanic Rift Zone

INEL-1 +

Big Lost River

Outline of ring fracture zone of inferred caldera

ANL

Central Facilities Area, INEL

Middle Butte

East Butte

Unnamed dome

ESRP

Arco Volcanic Rift Zone

Long axis

U.S. Highway 20

Big Southern Butte

112°45' W.

| 5 | 0 | 5 | 10 | 15 | 20 |

Kilometers

fans are middle Pleistocene to Holocene and many are cut by range-front faults.

Well-sorted and -bedded clay and silt were deposited on the floors of Pleistocene and Holocene lakes formerly located in the closed basins. Shoreline, bar, and beach deposits of gravel, sand, and silt occur along the margins of the old lakes, which were formed chiefly during the time of Pinedale Glaciation. Eolian deposits of well-bedded and stratified sand occur in longitudinal and transverse dunes located chiefly to the northeast (downwind) of the source areas of lake floor deposits.

Playa deposits of sand, silt, and clay occur in widely scattered depressions in other surficial deposits and in low areas in lava-covered terrane that are intermittently flooded.

Older lava flows in the map area are locally covered by as much as 10 m of loess, eolian sand, and alluvial deposits. Younger flows are covered by scattered accumulations of loess and eolian sand less than several meters thick (Kuntz and others, 1979).

Mountains North of the ESRP

Basin-range structures

Basin-range structure in the western United States consists of block-faulted mountain ranges and intervening alluviated valleys. The mountain region north of the Lava Ridge-Hells Half Acre map area conforms to this definition. A currently accepted model (Stewart, 1978) suggests that basin-range structure is produced by fragmentation of an upper crustal, brittle slab which overlies a plastically extending mantle. The extension causes the slab to be pulled apart along systematically spaced normal faults, causing the downdropping of horizontal prisms (graben) and the relative uplifting of horizontal prisms (horsts).

The Lost River, Lemhi, and Beaverhead Ranges are bounded by range-front, normal faults along their western margins. Range-front faults are absent or less strongly developed on the eastern margins of these ranges. The Howe fault forms a scarp as much as 12 m (40 ft) high in bedrock and alluvial-fan deposits along the west side of the Lemhi Range (fig. 2). Malde (1971) stated that at least 3 m (10 ft) of movement occurred on the Howe fault north of Berenice (fig. 2) less than 30,000 yrs ago and possibly less than 4,000 yrs ago based on offsets of alluvial deposits.

Segments of the Arco fault on the west side of the Lost River Range form prominent scarps in alluvial-fan deposits that may be as young as 10,000 yrs old, but other segments of the fault are covered by unbroken surficial deposits judged to be about 4,000 yrs old (Malde, 1971). Hait and Scott (1978) cited geomorphological evidence for about 2 m of displacement less than 12,000 yrs old on a segment of the Arco fault located 40-75 km north of Arco (fig. 1).

The Beaverhead fault on the west side of the Beaverhead Range disrupts drainage at the range front and beheads alluvial fans near Leadore, approximately 80 km north of the ESRP (Ruppel, 1964; fig. 1, this report). Although the time of latest movement on the Beaverhead fault has not been documented, it may correspond to the latest age of movement on the Howe and Arco faults.

An active fault may be defined as a break in the Earth's crust along which there has been recurrent movement in the recent geologic past (<20 m.y.) and along which there is likely to be movement in the future (Gary and others, 1972). A capable fault is an active fault that has had at least one rupture in the last 35,000 yrs and recurrent displacements in the last 500,000 yrs based on criteria used by the U.S. Nuclear Regulatory Commission (10CFR100,

Appendix A, paragraph III (g)). The geological evidence currently available for the normal faults along the range fronts of the mountains north of the Lava Ridge-Hells Half Acre area suggests that each may be termed an active fault and a capable fault.

The southern tips of the Lost River, Lemhi, and Beaverhead Ranges have abrupt, steep terminations, suggesting that the terminations may be controlled by a boundary fault or fault system along the northwest margin of the ESRP. Normal faults that have east to northeast trends, lengths of about 3 km (2 mi) or less, and displacements of about 15-30 m (40-80 ft) (Betty Skipp, oral. commun., 1979) cut bedrock and Pliocene and older(?) fan gravels in the southern part of the Lemhi and Beaverhead Ranges. The east-to northeast-trending faults are roughly parallel to the northwestern margin of the ESRP, but their lengths, displacements, and scattered distribution suggest that they do not constitute boundary faults or parts of a boundary fault system for this segment of the northwest margin of the ESRP. In addition, other scarps, alinement of volcanoes, and other geologic evidence for a boundary fault system are absent. If such a boundary fault system exists, it must lie several kilometers southeast of the physiographic border of the ESRP, where it is deeply buried by surficial deposits and lava flows.

Stratigraphy and thrust faults

The geology, stratigraphy, and structure of rocks within the mountain ranges on the northwest margin of the ESRP have been described only within the last few years as a result of field mapping chiefly, but not exclusively, by Betty Skipp, M. H. Hait, Jr., H. J. Prostka, and E. T. Ruppel of the U.S. Geological Survey; Robert Scholten and his students of the Pennsylvania State University; and E. C. Beutner of Franklin and Marshall College. Their studies show that the mountains consist mainly of upper Precambrian and Paleozoic sedimentary rocks, comprising limestones, dolomites, and shales that were

deposited in a miogeosynclinal environment. Skipp and Hait (1977) believed

that these rocks occur in at least nine major allochthons east of the Idaho

batholith, with each allochthon separated from the adjacent allochthon by

thrust faults. The allochthons are broken by younger Tertiary and Holocene

range-front, normal faults which impart the basin-range structure to the

block-fault mountains and intervening valleys north of the ESRP. Details of

the stratigraphy and structure of the mountains are not pertinent to this

report; they are discussed by Beutner (1968), Scholten (1957, 1973), Skipp and

Hait (1977), and Ruppel (1978).

BASALT VOLCANOES, LAVA FLOWS, AND MAGMAS

Basalt volcanism produces similar structures and landforms throughout the

world. Many of the volcanic structures and landforms observed on the ESRP are

similar to those formed in historic time on the island of Hawaii. Hawaiian

volcanic eruptions have been observed and documented by volcanologists for

about the last 75-100 yrs. Because basalt volcanism poses the greatest

volcanic hazard in the ESRP and because of the similarity between volcanic

products and processes in Hawaii and in the ESRP, an Appendix describing

eruptive processes and products in basalt volcanism, with examples drawn

largely from Hawaiian eruptions, is included in a previous paper by Kuntz

(1978b) and should be consulted by interested readers.

Geomorphology of volcanoes

Volcanoes in the Lava Ridge-Hells Half Acre area are chiefly of the

shield type. Shield volcanoes are broad, dome-shaped, gently sloping cones

(typically less than 5°) built up by the accumulation of hundreds or thousands

of individual pahoehoe lava flows and flow units and, rarely, aa lava flows,

all of which move relatively unexplosively and radially away from the summit

vent area. Areas covered by lavas erupted from three of the largest volcanoes

in the Lava Ridge-Hells Half Acre area are given in table 1. The high

Table 1.--Areas covered by lava flows of the Hells Half Acre, Kettle Butte, and Microwave Butte lava fields

Lava field	Area covered by lavas (km^2)
Hells Half Acre	430
Kettle Butte	[1] 320
Microwave Butte	[1] 270

[1] Figures cited are minimum estimates because distal flows are covered by surficial deposits.

See Kuntz and others (1979) and LaPoint (1977) for location of these lava flows.

fluidity (viscosity of about 1-100 poise) of pahoehoe lava flows allows them to advance at speeds of as much as several kilometers/hour down slopes of 5° or less; thus, they spread widely and cool as thin, nearly horizontal sheets approximately 5-10 m thick. The maximum length of lava flows from three of the largest shield volcanoes in the Lava Ridge-Hells Half Acre area is listed in table 2. Future eruptions in the Lava Ridge-Hells Half Acre area from large shield volcanoes are likely to produce lava flows that will inundate areas and reach lengths similar to those cited in tables 1 and 2.

Flow of lava away from a vent during early stages of eruption generally takes place through leveed channels. Large accumulations of pahoehoe lava formed during periods of high volume of effusion are typically fed by flow of lava through tubes and tube systems. In the Lava Ridge-Hells Half Acre area, leveed channels are found at Deuce Butte, Little Butte, Topper Butte, and Gil Butte volcanoes; lava tubes occur to the east and south of the vent area at Hells Half Acre volcano and southwest and west of the vent area at Microwave Butte volcano. (See Kuntz and others, 1979, for these geographic locations and those described below).

Volcanic vents in the Lava Ridge-Hells Half Acre area display shapes and structures suggesting that they were produced by a variety of volcanic processes. Many summits of volcanoes are indented by elongated, slot-shaped vent depressions (Tanner Butte, Little Butte, Gil Butte, Deuce Butte, and Hells Half Acre volcanoes) which overlie a feeder fissure(s). Other vent depressions are nearly circular in outline (unnamed vent between Kettle Butte and Tanner Butte, unnamed vent between Little Butte and Microwave Butte, unnamed vents on Lava Ridge) and are not easily related to a feeder fissure(s). Large deposits of cinders accumulated within 0.5 km of the vents at Little Butte and Microwave Butte, indicating that mildly explosive eruptive activity occurred at these vents and probably at other vents as well.

Table 2.--<u>Length of lava flows from large shield volcanoes in the Lava Ridge-</u>
<u>Hells Half Acre area</u>

Shield volcano	Maximum length of lava flows from vent (km)
Hells Half Acre	28
Microwave Butte	$\underline{1}/$ 24
Kettle Butte	$\underline{1}/$ 22

$\underline{1}/$ Figures cited are minimum values because distal flows are covered by surficial deposits.

See Kuntz and others (1979) and LaPoint (1977) for location of these lava flows.

Small calderas are steep-sided craters at a vent area that include smaller vents and pit craters. They are formed by collapse or explosive destruction of the summit vent area or both. Small calderas occur at Hells Half Acre and Kettle Butte volcanoes.

Two types of lava ponds occur in the Lava Ridge-Hells Half Acre area: (1) lava ponds formed by the filling of caldera or vent craters (Hells Half Acre vent area), and (2) perched lava ponds formed by ponding of lavas behind natural levees (Microwave Butte and Dome Butte volcanoes).

Lava flows

Most pahoehoe lava flows in the Lava Ridge-Hells Half Acre area consist of three gradational structural units (Kuntz, 1978a): (1) a thin (typically <2 m) top layer of fine-grained, vertically and horizontally jointed, vesicular, and locally clinkery basalt, (2) a thick (typically 5-7 m), central, massive layer consisting of coarser grained, typically diktytaxitic, lava with prominent vertical columnar joints and vesicle pipes, and (3) a thin (typically <1 m) basal layer consisting of fine-grained, scoriaceous blocks of lava that are typically oxidized.

The surfaces of younger pahoehoe lava flows are hummocky, with pressure plateaus and ridges, flow ridges and gutters, and collapse depressions. The accumulation of loess and eolian sand in depressions on older flows inparts a smooth surface, and only the higher features on the flows project through the cover of surficial deposits.

Petrography

The petrography of basalts in the Lava Ridge-Hells Half Acre area is relatively simple and described here in a summary manner. Most thin sections studied are of porphyritic basalt with phenocrysts of olivine and plagioclase, 0.5 to 2.0 mm in longest dimension, set in a matrix of olivine, plagioclase, clinopyroxene, ilmenite, magnetite, apatite, and glass, all less than 0.5 mm in longest dimension.

A few rocks are more strongly porphyritic, with olivine and plagioclase phenocrysts as much as 2 cm long, and a few rocks also display glomeroporphyritic clots of olivine and plagioclase as large as 2 cm in diameter. Nearly all rocks examined are intergranular and diktytaxitic to some degree, and some rocks display ophitic to subophitic textures. Alteration of glass to chlorophaeite and alteration of iron-bearing minerals to iron oxides are weakly to moderately developed in some samples. Silica minerals, alkali feldspars, and feldspathoids have not been observed in any thin sections of basalt lavas of the Lava Ridge-Hells Half Acre area.

Olivine phenocrysts are optically unzoned with an average composition of Fo_{65}. Small olivine crystals in the matrix are also optically unzoned and have an average composition of Fo_{55}. Many of the larger phenocrysts have square- or rectangular-shaped, isotropic inclusions believed to be chromium-rich spinel, based on the studies of Leeman and Vitaliano (1976). Olivine phenocrysts display a variety of shapes, including equant, rectangular, bladelike, and skeletal forms.

Plagioclase phenocrysts are typically normally zoned from cores of An_{65} to rims of An_{50}. Most crystals are tabular in shape, and many thin sections show a subparallel orientation of the larger laths. Plagioclase crystals with sieved textures and glomeroporphyritic clusters of plagioclase and olivine crystals are common. Bent and broken crystals and wavy extinction suggest that plagioclase crystals were intratelluric and were deformed prior to eruption and flow.

The clinopyroxene in all thin sections examined is light brown, shows very weak absorption, and has optical properties typical of augite. Blades of ilmenite and crystals of magnetite are common inclusions in clinopyroxene crystals. Nearly all of the clinopyroxene occurs in intergranular arrangement with plagioclase crystals. Larger crystals of clinopyroxene with subophitic and ophitic textures are rare. Neither orthopyroxene nor pigeonite were observed in any thin section studied from rocks of the Lava Ridge-Hells Half Acre area.

Chemistry

Chemical analyses of 17 basalts from large volcanoes in the Lava Ridge-Hells Half Acre area are listed in table 3. The analyses show a moderate amount of variability, some of which may be due to the different analytical methods used and the different laboratories in which the analyses were made. However, all 17 of the analyzed rocks are tholeiites in the normative component classification of Yoder and Tilley (1962). Specifically, 16 of the rocks are undersaturated olivine tholeiite (normative olivine and hypersthene) and one (Kettle Butte, Sample No. 6-14-6) is an oversaturated olivine tholeiite (normative quartz and hypersthene). Thus, in terms of both modal and normative mineral components, basalts of the Lava Ridge-Hells Half Acre area can be termed olivine tholeiites.

Table 3.—Chemical analyses and CIPW normative minerals of basalts from the Lava Ridge-Hells Half Acre area, eastern Snake River Plain, Idaho

		1	2	3	4	5	6	7	8	9	10	11
Location		Richard Butte	Lava Ridge	Antelope Butte	Circular Butte	Teat Butte	Dome Butte	Topper Butte	Vent 5316 Kettle Butte NW	Little Butte	State Butte	Middle Butte
Field Sample No.		MAK76-S125	MAK76-S127	MAK76-S119	MAK76-S133	MAK76-S134	MAK76-S177	MAK76-S176	MAK76-S169	MAK75-S223A	MAK76-599	72S24
USGS Lab. Sample No.		M-133718	M-133691	M-133682	M-133683	M-133703	M-133684	M-133694	M-133687	W-192048	M-133688	W-179477
Collected by		M. A. Kuntz	M. A. Kuntz	M. A. Kuntz	M. A. Kuntz	M. A. Kuntz	M. A. Kuntz	M. A. Kuntz	M. A. Kuntz	M. A. Kuntz	M. A. Kuntz	G. T. Stone

Chemical analyses

		1	2	3	4	5	6	7	8	9	10	11
SiO_2		45.60	46.17	47.28	47.47	46.35	46.38	46.24	46.60	47.1	46.34	47.1
TiO_2		3.29	3.16	2.36	3.46	2.58	3.48	3.48	2.77	2.1	2.96	2.9
Al_2O_3		15.56	15.33	15.21	13.56	15.65	14.78	14.73	15.26	15.6	15.04	16.1
Fe_2O_3		2.42	2.45	1.72	0.92	3.58	2.59	3.94	2.39	1.9	3.68	3.1
FeO		12.28	12.11	11.13	13.64	9.89	12.41	11.63	11.30	10.2	10.35	10.4
MnO		.19	.20	.19	.23	.20	.21	.21	.20	.15	.21	.14
MgO		6.09	7.30	8.10	7.37	7.99	6.61	6.57	6.94	8.3	7.04	6.2
CaO		9.60	9.89	10.14	10.07	10.03	9.39	9.38	9.73	10.7	10.33	9.5
Na_2O		2.87	2.83	2.67	2.53	2.92	2.62	2.73	2.71	2.5	2.83	2.9
K_2O		.55	.56	.67	.54	.67	.73	.72	.71	.44	.62	.70
P_2O_5		.99	.74	.58	1.18	.65	.81	.78	.83	.55	.84	.48
H_2O^+		.31	.30	.42	.36	.46	.40	.30	.32	.36	.27	.31
H_2O^-		.17	.08	.10	.06	.12	.06	.15	.12	.09	.10	.13
CO_2		--	--	--	--	--	--	--	--	--	--	0.08
Total		99.92	101.12	100.57	101.39	101.09	100.47	100.86	99.88	100.0	100.61	100.0
Method		XRF	XRF	XRF	XRF	XRF	XRF	XRF	XRF	RR	XRF	RR
Analyst		L. Espos	M. Villarreal	M. Villarreal	M. Villarreal	M. Villarreal	L. Espos	M. Villarreal	M. Villarreal	Z. A. Hamlin	M. Villarreal	Unknown

CIPW normative minerals

		1	2	3	4	5	6	7	8	9	10	11
Q		--	--	--	--	--	--	--	--	--	--	--
Or		3.25	3.27	3.94	3.15	3.92	4.29	4.22	4.20	2.60	3.64	4.14
Ab		24.31	23.68	22.47	21.12	24.44	22.07	22.90	22.96	21.16	23.80	24.55
An		27.97	27.17	27.38	23.72	27.32	26.29	25.59	27.41	30.05	26.34	28.85
Di:		10.94	13.64	15.48	14.87	14.39	12.22	12.71	12.74	15.89	15.62	12.44
Wo		5.52	6.92	7.88	7.49	7.39	6.18	6.47	6.47	8.12	7.99	6.33
En		2.69	3.64	4.30	3.62	4.46	3.13	3.51	3.41	4.63	4.61	3.43
Fs		2.74	3.08	3.30	3.75	2.54	2.91	2.73	2.87	3.13	3.02	2.67
Hy:		9.09	4.94	5.47	17.20	1.97	13.94	13.31	10.49	8.25	7.20	10.57
En		4.50	2.68	3.12	8.45	1.26	7.23	7.48	5.69	4.92	4.35	5.95
Fs		4.59	2.26	2.55	8.75	.71	6.72	5.83	4.80	3.33	2.85	4.62
Ol:		11.90	15.79	16.08	9.04	15.93	8.55	6.82	11.10	13.59	10.21	7.89
Fo		5.60	8.17	8.72	4.22	9.79	4.22	3.67	5.75	7.79	5.93	4.25
Fa		6.30	7.61	7.37	4.82	6.13	4.32	3.15	5.35	5.80	4.28	3.64
Mt		3.51	3.51	2.48	1.32	5.14	3.74	5.66	3.47	2.76	5.30	4.50
Il		6.25	5.94	4.46	6.48	4.85	6.58	6.55	5.27	3.99	5.59	5.51
Ap		2.35	1.73	1.37	2.76	1.52	1.91	1.83	1.97	1.30	1.98	1.14

Table 3. (cont.)--Chemical analyses and CIPW normative minerals of basalts from the Lava Ridge-Hells Half Acre area, eastern Snake River Plain, Idaho

	12	13	14	15	16	17	Mean and standard deviation of analyses 1 through 17		
Location	Vent 5421 Middle Butte quad.	Kettle Butte	Kettle Butte	Vent 5238 Butterfly Butte quad.	Butterfly Butte	Hells Half Acre			
Field Sample No.	MAK75-S225	6-14-6	6-27-86	6-15-8	MAK76-S83	6-16-6	$\bar{x}$	σ	RSD[1]
USGS Lab Sample No.	W-192046	W-190342	-----	----	M-133713	W-190343			
Collected by	M. A. Kuntz	J. Karlo	J. Karlo	J. Karlo	J. Karlo	J. Karlo			

Chemical analyses

	12	13	14	15	16	17	$\bar{x}$	σ	RSD
SiO_2	46.4	47.5	44.27	44.68	45.18	48.4	46.41	1.06	2.3
TiO_2	3.7	3.2	3.39	3.30	3.08	2.9	3.07	0.43	14.0
Al_2O_3	14.9	15.5	13.88	14.92	15.22	15.3	15.09	0.62	4.1
Fe_2O_3	2.1	2.9	1.99	0.89	1.80	2.9	2.43	0.87	35.8
FeO	13.2	11.6	14.79	15.00	13.10	12.6	12.10	1.52	12.6
MnO	0.18	0.22	0.22	0.25	0.20	0.22	0.20	0.03	15.0
MgO	6.6	4.9	5.15	6.69	7.80	6.5	6.83	0.95	13.9
CaO	9.5	9.5	9.86	8.50	9.20	8.5	9.64	0.57	5.9
Na_2O	2.5	2.7	2.47	2.77	2.83	2.5	2.70	0.15	5.6
K_2O	0.49	0.74	0.77	0.73	0.61	0.82	0.65	0.11	16.9
P_2O_5	0.81	1.1	1.85	1.13	0.78	0.54	0.86	0.33	38.4
H_2O^+	0.49	0.35	0.34	0.30	0.09	0.25	0.33	0.09	27.3
H_2O^-	0.09	0.15	—	—	0.02	0.03	—	—	--
CO_2	0.01	0.25	0.34	0.25	--	0.07	—	—	—
Total	101.0	100.6	99.38	99.92	99.91	101.53	100.31		
Method*	RR	RR	XRF	XRF	XRF	RR			
Analyst	Z. A. Hamlin	S. Botts	J. Karlo	J. Karlo	L. Espos	S. Botts			

CIPW normative minerals

	12	13	14	15	16	17	$\bar{x}$	σ	RSD
Q	—	0.60	—	—	--	--	—	—	--
Or	2.87	4.36	4.60	4.35	3.61	4.78	3.83	0.63	16.4
Ab	20.95	22.77	21.12	23.64	23.97	20.86	22.75	1.32	5.8
An	27.72	22.89	24.76	26.34	27.05	27.71	26.74	1.77	6.6
Di	11.36	9.90	10.46	7.30	11.17	8.60	12.33	2.49	20.2
Wo	5.73	4.97	5.20	3.65	5.65	4.34	6.25	1.30	20.8
En	2.79	2.29	2.04	1.58	2.87	2.12	3.24	0.93	28.7
Fs	2.83	2.64	3.23	2.07	2.64	2.14	2.84	0.41	14.4
Hy	17.61	21.21	15.48	6.74	1.71	24.71	11.19	6.53	58.3
En	8.73	9.87	5.99	2.92	0.89	12.29	5.68	3.09	54.4
Fs	8.88	11.34	9.49	3.82	0.82	12.42	5.52	3.55	64.3
Ol	7.08	—	9.50	21.07	22.12	2.30	11.11	5.90	53.1
Fo	3.34	—	3.46	8.62	10.99	1.09	5.62	3.04	54.0
Fa	3.74	—	6.04	12.45	11.13	1.21	5.49	3.10	56.5
Mt	3.02	4.19	2.92	1.30	2.61	4.15	3.50	1.25	35.7
Il	6.96	6.06	6.51	6.32	5.86	5.43	5.80	0.81	14.0
Ap	1.90	2.60	4.43	2.70	1.85	1.26	2.03	0.79	38.9

* XRF, X-ray fluorescence (Fabbi and Espos, 1976); RR, rapid rock (Shapiro, 1975)

[1] RSD, relative standard deviation. RSD (%) = $\frac{\text{Standard Deviation} \times 100}{\text{Mean}}$

The average of the 17 analyses in table 3 is compared with averages of various types of tholeiites in table 4. These data show several distinctive chemical features of the olivine tholeiites of the Lava Ridge-Hells Half Acre area: (1) they are significantly lower in SiO_2, and (2) they are significantly higher in TiO_2, total iron, and P_2O_5, when compared to the average tholeiite analyses. These distinctive chemical features apply equally well to nearly all basalts of the Snake River Plain (Stone, 1967), and therefore these rocks form a unique chemical suite of basalts.

The distinctive chemical features are reflected in the mineralogy of Snake River Plain tholeiites. The low silica content is reflected in large amounts of modal olivine (generally greater than 10 percent) and the absence of silica minerals. The high titanium and total iron content are reflected in large modal amounts of ilmenite and titanomagnetite and relatively iron-rich olivine and pyroxenes. The significantly large amounts of P_2O_5 are reflected in ubiquitous apatite crystals.

Petrogenesis

Recent studies (Stone, 1967; Tilley and Thompson, 1970; Thompson, 1975; Leeman and Vitaliano, 1976; and Stout and Nicholls, 1977) of the petrogenesis of the olivine tholeiite lavas of the Snake River Plain, based largely on experimental, chemical, and petrographic data, have all reached similar and consistent conclusions; namely: (1) the most magnesium-rich, aphyric rocks represent "primary magmas," (2) the magmas were formed by approximately 15-20 percent partial melting of a spinel lherzolite mantle source at pressures of 15-20 kbar and at temperatures of approximately $1300^\circ C$ under anhydrous or nearly anhydrous (≤ 2 percent H_2O) conditions, (3) partial crystallization and fractionation of olivine and plagioclase and, to a lesser extent, clinopyroxene at <8 kbar gives rise to more fractionated rocks such as

Table 4.--Comparison of the average chemical composition of 17 basalts from the Lava Ridge-

Hells Half Acre area with various average compositions of tholeiitic basalts

	Average of 17 basalts from Lava Ridge-Hells Half Acre area (table 3 this report)	Average of 282 oceanic tholeiites (Manson, 1967, Table IV)	Average of 946 continental tholeiites (Manson, 1967, Table IV)	Average of 182 olivine tholeiites (Manson, 1967, Table II, column 8)
SiO_2	46.4	49.3	51.5	48.6
TiO_2	3.1	2.4	1.2	1.7
Al_2O_3	15.1	14.6	16.3	15.5
Fe_2O_3	2.4	3.2	2.8	2.6
FeO	12.1	8.5	7.9	8.7
MnO	.20	.17	.17	.17
MgO	6.8	7.4	5.9	8.4
CaO	9.6	10.6	9.8	10.3
Na_2O	2.7	2.2	2.5	2.3
K_2O	.65	.53	.86	.6
P_2O_5	.86	.26	.21	.23
H_2O^+	.33	.79	.81	.9
Total	100.2	100.0	100.0	100.0

22

tholeiitic andesite, and (4) the lavas were erupted at temperatures of about 1200°C.

Studies by Hill and Pakiser (1967), Mabey (1976), and Stout and Nicholls (1977) suggest that the crustal structure of the WSRP comprises four distinct layers: (1) a composite layer of sediments, basalt flows, and silicic volcanic rocks as much as 8 km thick having densities ranging from 2.25 g/cm^3 to 2.9 g/cm^3; (2) an upper crustal "granitic" layer 8-10 km thick that has an average Vp of 5.2 km/sec and assumed density of 2.65 g/cm^3, which is greatly thinned (and may be completely rifted) when compared to similar crust in adjoining areas; (3) a lower crustal "basaltic" layer 34-38 km thick that has an average Vp of 6.7 km/sec and assumed density of 3.0 g/cm^3; below which lies (4) mantle with an average Vp of 7.9 km/sec. The Moho in the WSRP has an average depth of about 45 km. The top of a low-velocity zone in the upper mantle in the WSRP is located at approximately 60 km.

The crustal structure of the ESRP has been determined with certainty only recently through the studies of Mabey (1978), Stanley and others (1977), and Braile (1978). The crust beneath the ESRP between Arco and Blackfoot consists of three layers: (1) a composite layer of continental sediments, basalt lava flows, and rhyolite ash flows and lava flows that are $\leq$ 2 km thick; 2) an upper "granitic" crust about 15 km thick that has an average Vp of 6.2 km/sec and an assumed density of 2.7 g/cm^3, consisting chiefly of rhyolitic, granitic, and granulitic rocks; and (3) a lower "basaltic" crust about 13 km thick that has an average Vp of 6.5 km/sec and an assumed density of 3.0 g/km^3. The three crustal layers yield an aggregate thickness of about 28-30 km. Gravity models suggest a considerable amount of crustal thinning to the northeast toward the Yellowstone Plateau, where the depth to the Moho may be as shallow as 20 km. No seismic evidence currently available indicates a

low-velocity zone in the upper mantle beneath the ESRP, but magnetotelluric studies by Stanley and others (1977) indicated that temperatures in excess of $900^{\circ}C$ are present in the upper mantle, suggesting that a low-velocity layer or zone of partial melting can be reasonably inferred.

It is interesting to compare the depths to boundaries of the crustal layers described above and the depths at which significant petrologic processes inferred in the formation of basaltic magmas occur. The low-velocity zone of 60 km beneath the WSRP corresponds to the zone of partial melting inferred from the experimental, chemical, and petrographic data. The inferred depth at which low pressure (<8 kbar) fractionation takes place is about 25-30 km, the depth of the base of the crust in the ESRP. If basaltic magmas rise buoyantly through the crust, as described by Leeman and Vitaliano (1976), they would reach a density-viscosity contrast at the crust-mantle (Moho) boundary which would likely slow their rate of rise and facilitate fractionation. Thus the magmas form at depths of approximately 60 km in the mantle and then rise to a holding reservoir produced by the density-viscosity contrast at the Moho at a depth of about 25-30 km, where low-pressure fractionation takes place. Perhaps emplacement of magmas at the surface and the distribution of volcanoes in volcanic rift zones is facilitated by faults in the crust. That faulting of the crust triggers subsequent volcanism implies that the faults provide favorable structures for continued buoyant rise of magma from the reservoir and that faulting produces or accompanies large deviatoric stresses in the lower crust that facilitate the rise. It seems clear that faults in the upper crust localize volcanoes at the surface along volcanic rift zones, but whether or not faulting or its effects initiate the rise of basaltic magma is unknown.

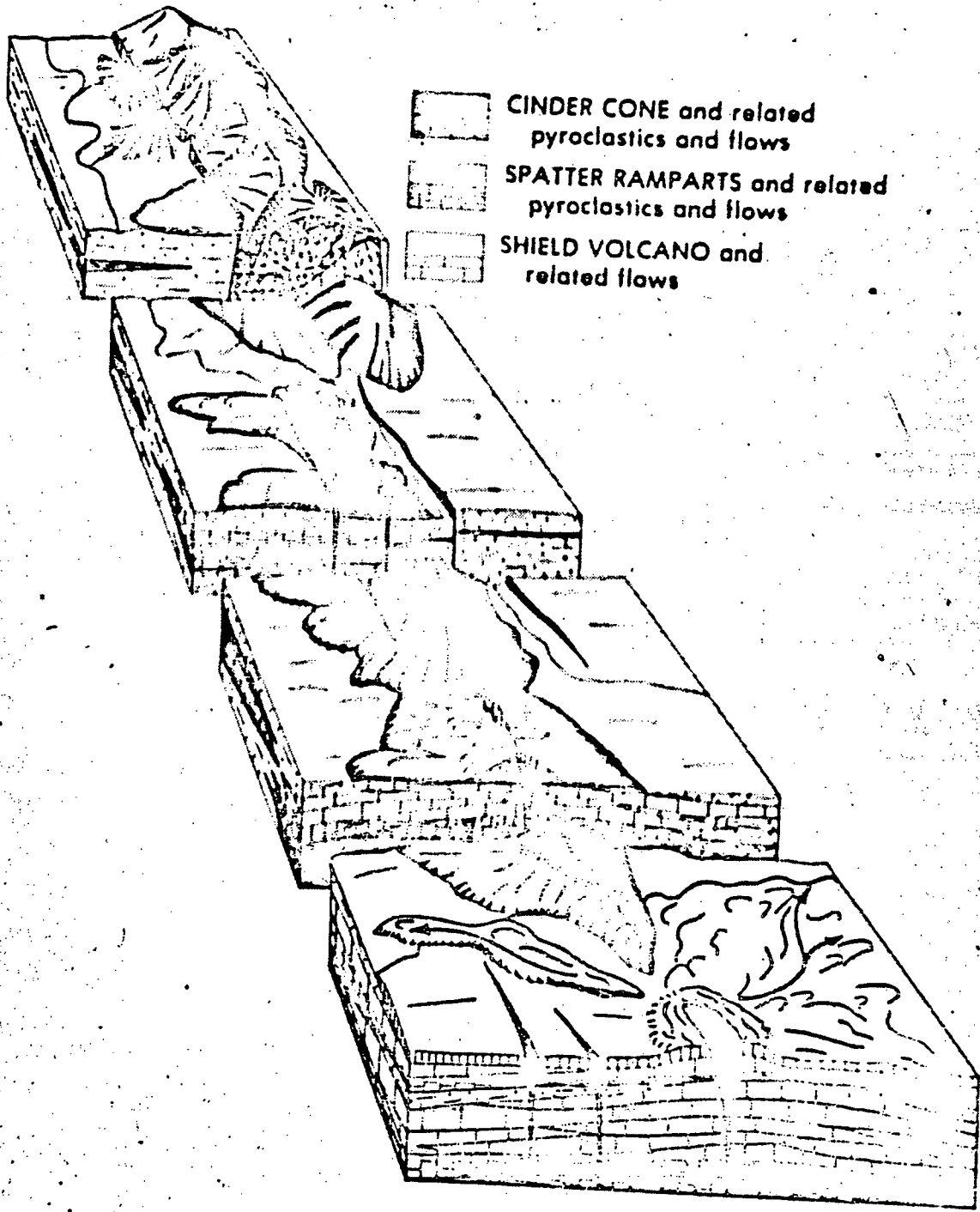VOLCANIC RIFT ZONES AND THEIR STRUCTURAL AND TEMPORAL RELATIONS

Volcanic rift zones of the ESRP are linear arrays of volcanic landforms and structures related to volcanism. The structures include open fissures, faults, and graben. The volcanic landforms include fissure flows, spatter ramparts, cinder cones, lava cones, and shield volcanoes. The vent depressions of cinder cones, lava cones, and shield volcanoes are typically elongated parallel to the volcanic rift zones, indicating that eruptive fissures influenced the size and shape of the vents. Figure 3 is a generalized diagram showing structures and volcanic landforms in an idealized volcanic rift zone in the central part of the ESRP.

Field studies by Kuntz (1977a, 1977b, 1977c) show that, in general, volcanic rift zones of the ESRP are extensions of range-front, normal faults and thrust faults beneath the plain, as shown diagrammatically in figure 3. Two volcanic rift zones which have localized volcanism in the vicinity of the ANLW facilities are the Lava Ridge-Hells Half Acre volcanic rift zone and the Circular Butte-Kettle Butte volcanic rift zone (fig. 2). The Lava Ridge-Hells Half Acre volcanic rift zone is an extension of the Howe fault, and the Circular Butte-Kettle Butte volcanic rift zone appears to be an extension of a poorly defined fault zone on the east side of the Lemhi Range. (See Kuntz and others, 1979, and fig. 2.)

Lava Ridge-Hells Half Acre volcanic rift zone

Available field and age data suggest that distinct segments of the Howe fault and the Lava Ridge-Hells Half Acre volcanic rift zone have experienced displacement and volcanism at various and probably unrelated times. Malde (1971) stated that the segment of the Howe fault north of Berenice (fig. 2) experienced faulting with purely vertical movement within the last 30,000 yrs and possibly within the last 4,000 yrs, but all volcanism nearby along the

Figure 3.—Diagrammatic representation of volcanic and structural features in
an idealized volcanic rift zone in the eastern Snake River Plain,
Idaho. A block-faulted mountain range is shown in purple; volcanic
deposits and volcanic landforms, in red, orange, and yellow; faults and
fissures, in black; a river blue, and surficial deposits, white and gray.

CINDER CONE and related
pyroclastics and flows

SPATTER RAMPARTS and related
pyroclastics and flows

SHIELD VOLCANO and
related flows

northwest end of the Lava Ridge-Hells Half Acre volcanic rift zone is
estimated to be older than 100,000 yrs (Kuntz and others, 1979).

The Hells Half Acre volcanic field is located over a part of the volcanic
rift zone marked by open fissures that reveal purely horizontal extension
(Kuntz and others, 1979). Lavas of the Hells Half Acre volcanic field (age
$4,100\pm200$ [14]C yrs, Meyer Rubin, U.S. Geological Survey, written commun., 1977)
cover the open fissures but are not broken above them. This relation suggests
that the magma which fed the Hells Half Acre lava field reached the surface
along a pre-existing fissure system.

The Lava Ridge-Hells Half Acre volcanic rift zone is offset in a right-
lateral sense along a north-south-trending fissure system southeast of the
ANLW facilities (fig. 2; Kuntz and others, 1979). Ruppel (1964) described
right-lateral offset of bedrock in the Lemhi, Beaverhead, and Lost River
Ranges and of their range-front faults along north-south strike-slip faults.
Perhaps the Lava Ridge-Hells Half Acre volcanic rift zone is offset by faults
with similar orientations that are located in the underlying crust.

As discussed in the next section much of the length of the Lava Ridge-
Hells Half Acre volcanic rift zone is believed to coincide with a ring-
fracture zone along the northeast margin of a buried rhyolite caldera
(fig. 2).

Circular Butte-Kettle Butte volcanic rift zone

The Circular Butte-Kettle Butte volcanic rift zone is poorly defined at
its northwestern end owing to a thick accumulation of alluvial deposits
located at the mouth of Birch Creek (Kuntz and others, 1979; fig. 2). The
magnetic polarity of lavas near Circular Butte is reversed; thus the lavas are
probably older than 700,000 yrs. The Circular Butte-Kettle Butte volcanic
rift zone southeast of Circular Butte (fig. 2) is characterized chiefly by
lavas that are judged to have been erupted between 400,000 and 700,000 yrs

ago, but lavas were erupted at a single vent at Kettle Butte probably less than 100,000 yrs ago (Kuntz and others, 1979). If magma delivery to the surface is temporally related to movement on range-front normal faults and their extensions in crustal rocks beneath volcanic rift zones, the relationships described in the previous section suggest that the southern end of the range-front normal fault on the east side of the Lemhi Range and its extension beneath the Circular Butte-Kettle Butte volcanic rift zone has been relatively inactive since middle Pleistocene time. Ruppel (1964) reached similar conclusions about the age of movement on a segment of the same fault located about 65 km northwest of the ESRP.

Implications of the structural-temporal relationships

Some important implications about the volcanic rift zones are; Range-front normal faults that have had recurrent movement in late Pleistocene-Holocene time are co-linear with volcanic rift zones that have experienced generally coeval volcanism, and, conversely, range-front normal faults that have experienced little or no displacement since middle Pleistocene time are co-linear with volcanic rift zones on which the volcanism is chiefly pre-middle Pleistocene in age. The implication of these relations is that the extension of a capable fault (displacement within the last 35,000 yrs and recurrent movement within the last 500,000 yrs) beneath lavas of the ESRP produces a volcanic rift zone with correspondingly young volcanism. Accurate estimates of the age of movement on range-front normal faults and the age of volcanism on nearby segments of a volcanic rift zone are not available to prove whether faulting triggers volcanism.

The orientation of northwest-trending segments of range-front normal faults and north-trending strike-slip faults that offset the range-front faults in the mountain ranges north of the ESRP is identical to the orientation of volcanic vents and fissures in the Lava Ridge-Hells Half Acre

volcanic rift zone. These structural relationships imply that volcanic rift zones are the surface expression of normal and strike-slip faults in upper crustal "basement" rocks beneath the volcanic-sediment cover of the ESRP. The relationship between the faults and volcanic rift zones suggests that the faults are vertical or nearly vertical structures that penetrate deeply into the crust, because the faults act as conduits for delivery of magma to the surface.

Another important implication is that part of the Lava Ridge-Hells Half Acre volcanic rift zone coincides with part of the ring-fracture zone of an inferred buried caldera. It seems reasonable to assume that basalt volcanism along this segment of the volcanic rift zone is facilitated by a structural zone of weakness generated by differential collapse on the ring fracture and by continued basin-range faulting.

In summary, the above data suggest a process involving magma generated in the mantle beneath the plain, which rises buoyantly through the mantle and lower crust, and reaches the surface at volcanic vents whose positions and orientations are controlled by faults bounding blocks in the upper crust or by caldera ring fractures.

Additional and even more fundamental implications regarding the volcanic rift zones are: (1) basin-range structure (chiefly fault-bounded crustal blocks) and possibly topography may locally underlie the 1,000-to 2,000-m-thick lava-sediment cover of the ESRP; (2) volcanic rift zones are not superposed over possible boundary faults parallel to the margins of the ESRP; on the contrary, they cut across possible boundary faults; (3) the extensional tectonism that distinguishes the basin-range mountains north and south of the ESRP also characterizes the plain, and, thus, the ESRP is subject to the same tectonic stresses that currently affect the basin-range areas north and south of the ESRP.

Implications 2 and 3 suggest that the ESRP is not structurally "decoupled" from the adjoining mountains.
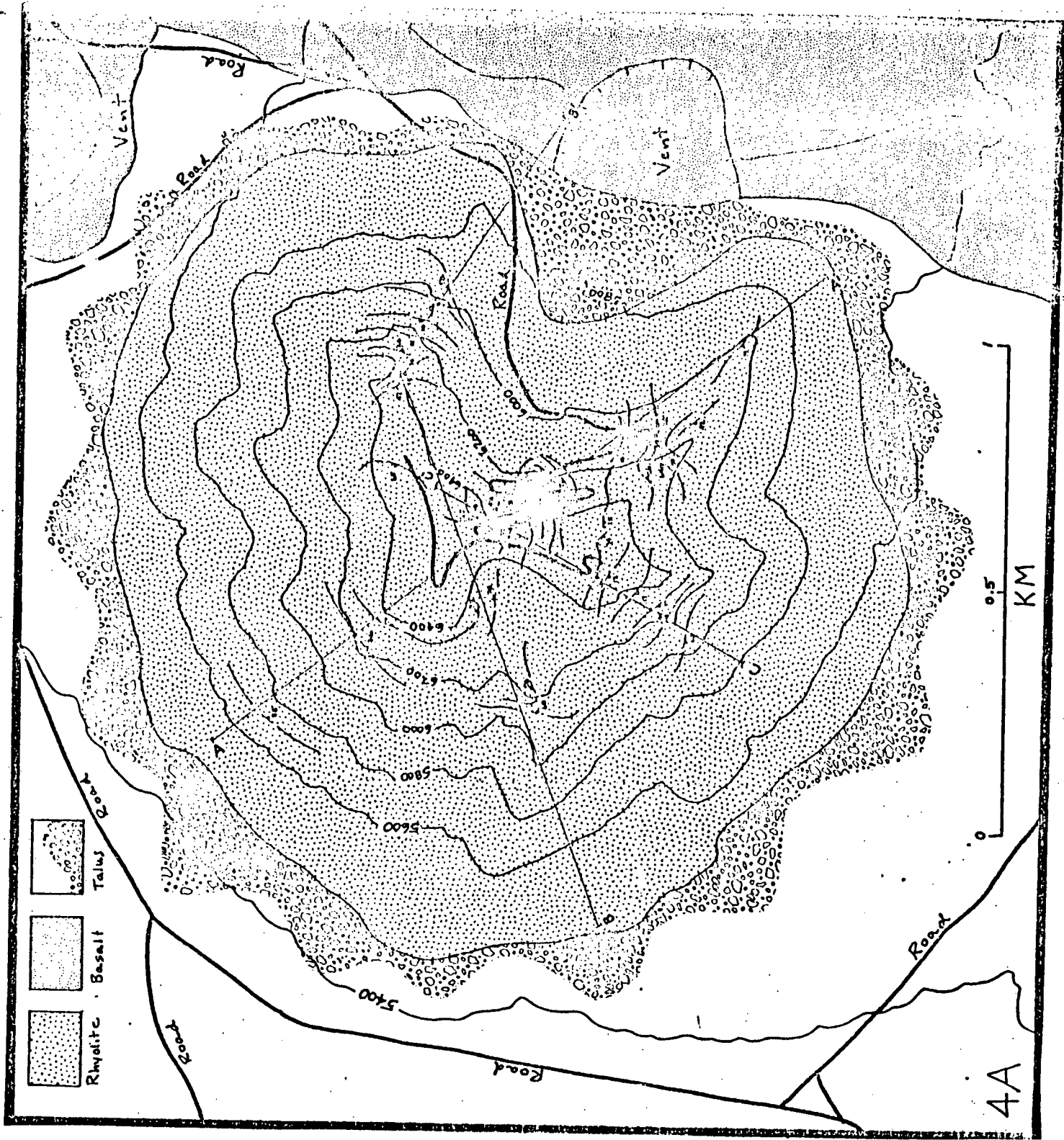
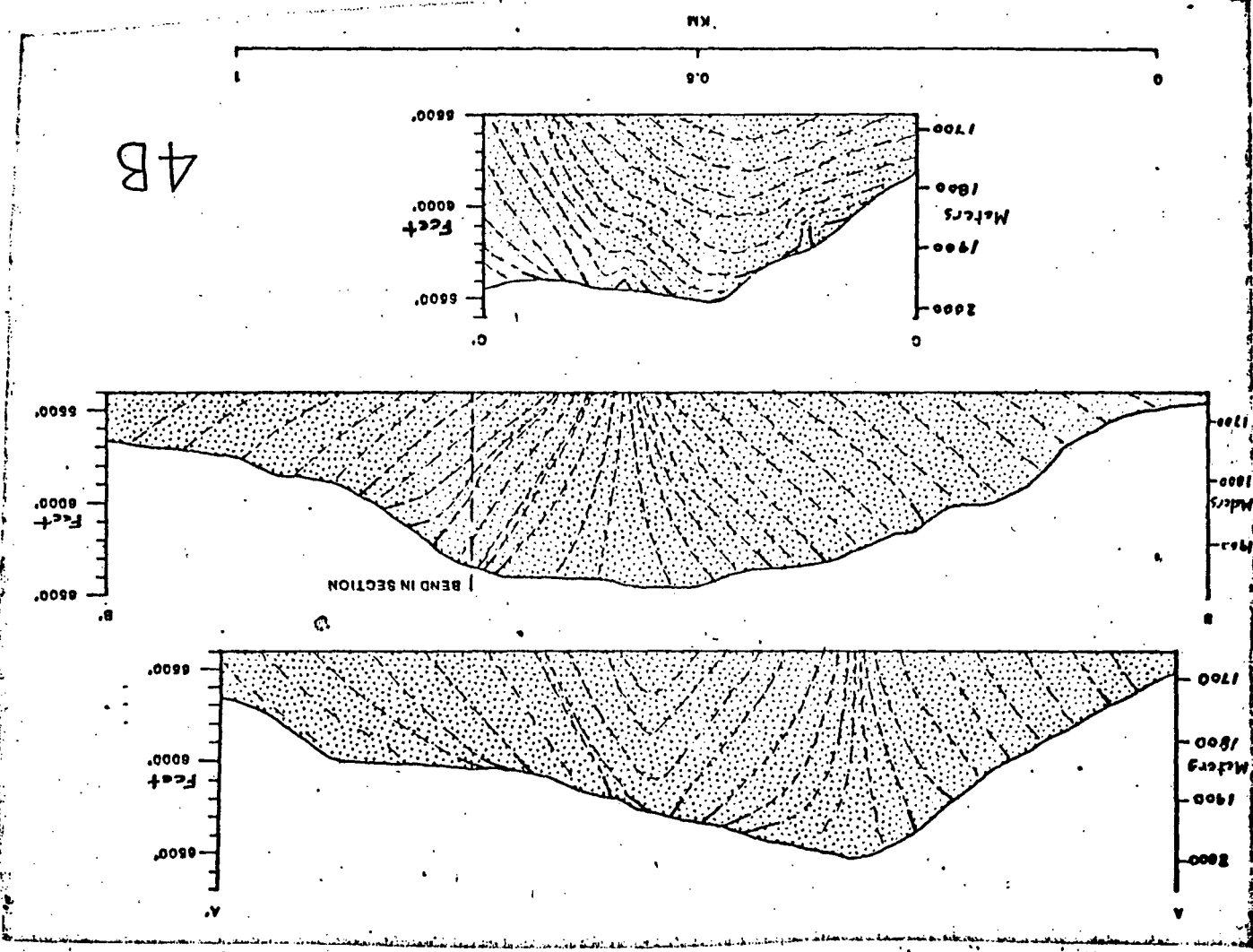## Rhyolite Domes

Field and structural relations

Three steep-sided hills, rising as much as 350 m above the surrounding basalt-lava-covered terrane, are prominent physiographic features in the southern part of the Lava Ridge-Hells Half Acre area. They are East Butte, Middle Butte, and a smaller, unnamed hill located about 1 km southwest of East Butte. (See Kuntz and others, 1979, and figs. 2 and 5A for locations.) Rhyolite lava flows and breccias are exposed at East Butte and the unnamed hill but not at Middle Butte. The steep sides of Middle Butte are covered by thick accumulations of talus composed of blocks that have been dislodged from the approximately 75-m-thick layer of basalt lava flows that cap the butte. However, magnetic and gravity data suggest that the core of Middle Butte consists of rock that is less dense and less magnetic than basalt, and is probably rhyolite (Don Mabey, USGS, oral commun., 1978). These factors and the structural data described below all indicate that the three hills are the upper parts of rhyolite domes.

The internal structure of East Butte is known from study of the orientation of the flow layering in its rhyolite lava flows (fig. 4). The flow banding generally defines inward-dipping, concentric layers similar to those of a short, stubby carrot or the lower half of an elongated onion. Flow layering parallel to an original upper surface is present in many rhyolitic domes (Williams, 1932), but is present only locally at East Butte. The orientation of the flow layering suggests that East Butte is a protrusion of a mass of lava that was too viscous to flow, and that the magma rose as inclined concentric sheets. Coulees, viscous lava flows that have blocky, steep-sided

Figure 4.--Orientation of flow layering in rhyolite lava flows of East

    Butte. A, generalized geologic map; B, cross sections. A-A´, B-B´, and

    C-C´.

Rhyolite   Basalt   Talus

0.5   KM

5700
5400
5500
5800
6000
6100
6200
6300
5600

Road
Road
Road
Road
Road
Vent
Vent

4A

4B

forms and that move radially away from a central vent, are absent at all three of the domes.

The exposed surface of East Butte is that of a nearly perfect gumdrop, except for a notch on its southeastern side. The notch lies opposite a large vent for a basalt volcano located in the SW 1/4, sec. 13, T. 2 N., R. 32 E. (See figures 4A and 5A.) Inclusions of basalt from this vent occur in the rhyolite of East Butte, indicating that the vent is older than the dome. These factors suggest that the rhyolite magma which formed the dome of East Butte was extruded from part of the same vent or fissure system that controlled the location of the basalt vent. Perhaps the rhyolite magma was protruded through a fissure that was partially blocked by basalt lava; the constriction would then have formed an obstruction to the extrusion of the rhyolite magma, resulting in formation of the notch on the southeast side of East Butte.

A geothermal exploration well, located in the NE 1/4, sec. 22, T. 2 N., R. 32 E. between East Butte and Middle Butte, was drilled to a depth of 610 m (2,000 ft) in the summer and fall of 1978 (Doherty, 1979). The well penetrated part of the unnamed rhyolite dome and revealed details of its petrology and structure. The upper 118 m (388 ft) of the well passed through at least 13 basalt lava flows that overlie the dome. Flow-banded and flow-brecciated, vitric to devitrified, dense rhyolite lava flows occur between depths of 118 m (388 ft) and 522 m (1,712 ft). The rhyolite is underlain by 87 m (288 ft) of dense, altered basalt flows. The well is believed to have penetrated the edge of the unnamed rhyolite dome, as shown in figure 5B. Both surface outcrops and parts of the core from the well display breccia containing fragments of rhyolite and pumice as much as 1 to 2 m in diameter set in a fine-grained, pumiceous matrix. The breccias probably formed by

Figure 5.—Geologic map (5A) and cross sections (5B) of Middle Butte, East

Butte and an unnamed rhyolite dome. Scale in 5B. Abbreviations on

Geologic map (5A): Qbc; basalt lava flows and related pyroclastic

deposits (middle Pleistocene—estimated to be 100,000 to 400,000 years

old). Qbd; basalt lava flows and related pyroclastic deposits (middle

Pleistocene—estimated to be 400,000 to 700,000 years old). Qbe; basalt

lava flows and related pyroclastic deposits (lower Pleistocene—older

than 700,000 years). Qr; rhyolitic lava flows and related flow breccia

(middle to lower Pleistocene). Qfc; poorly sorted fan deposits of

alluvium and colluvium (Holocene to middle Pleistocene). See Kuntz and

others (1979) for more detailed descriptions of map units.
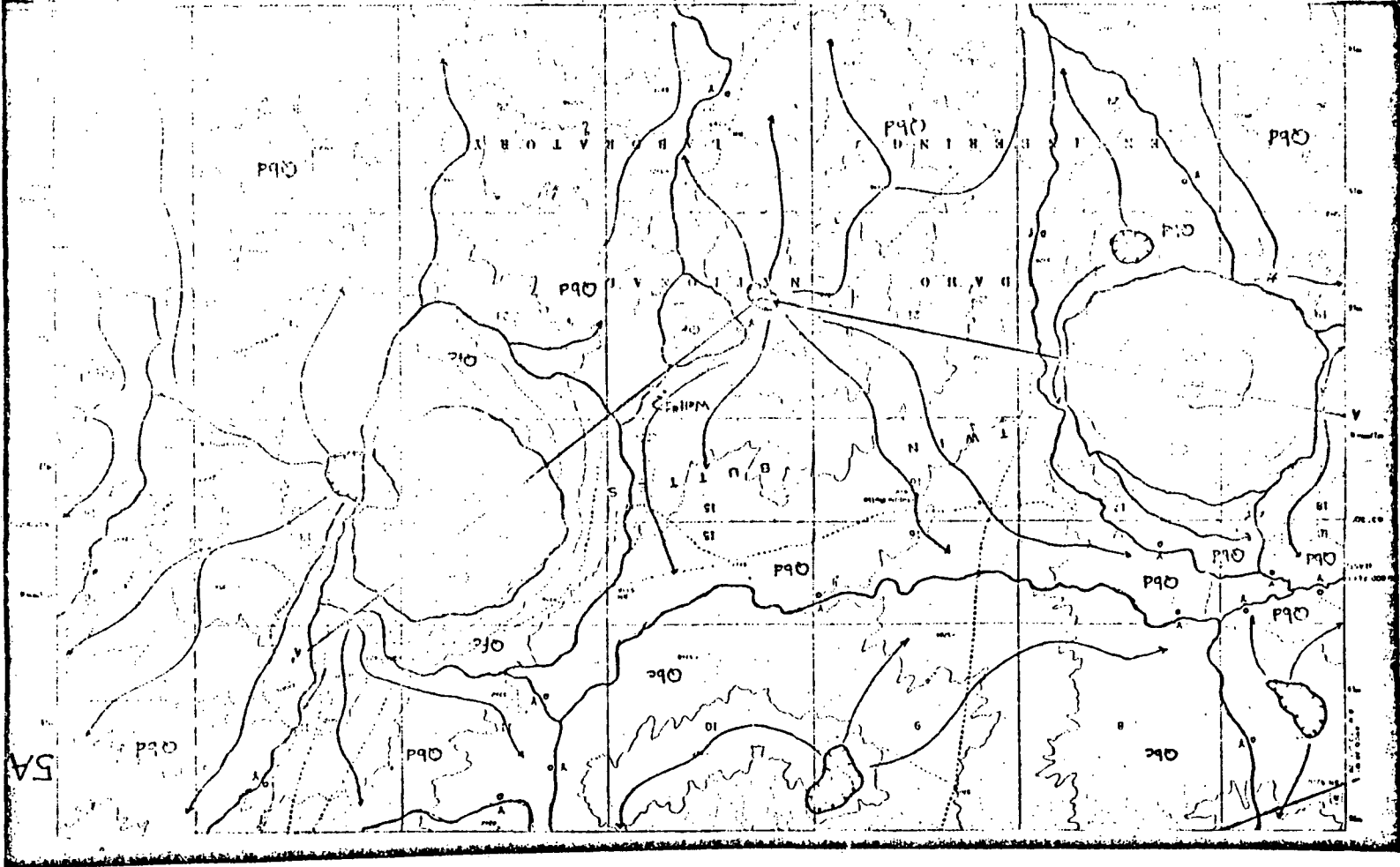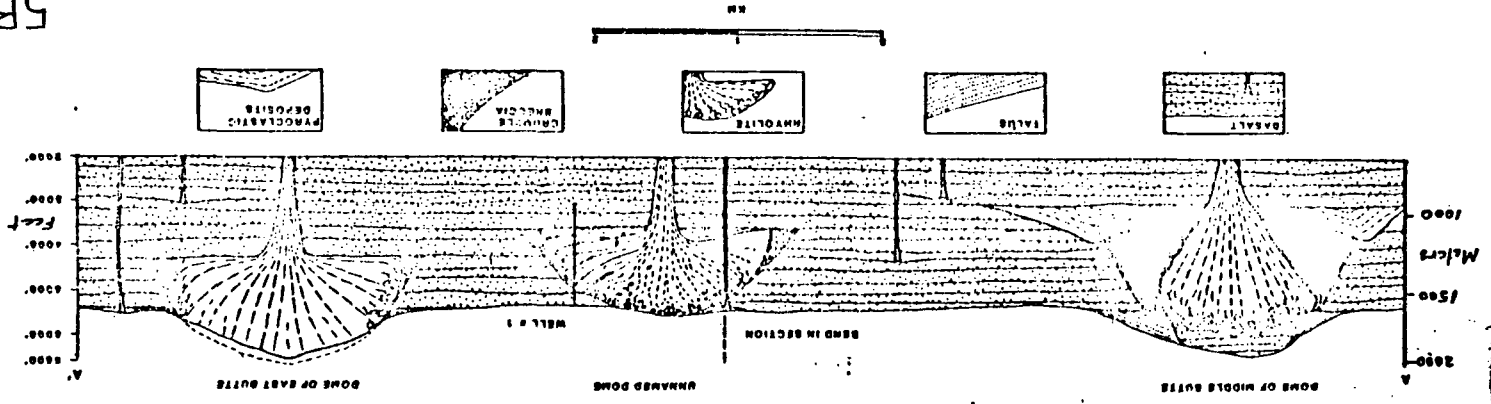
breakup of the outer crust and by frictional drag between layers of the dome
as it grew by internal expansion.

The basalt beneath the rhyolite is hydrothermally altered, and the base
of the rhyolite section consists of flow-banded rhyolite without breccia.
These factors suggest that the rhyolite flowed directly onto the upper surface
of a basalt flow and that the dome does not lie within a crater of previously
formed ash or lapilli.

The approximately 75-m-thick section of basalt lava flows atop Middle
Butte, the steep sides of this dome, and the absence of exposures of rhyolite
on the butte suggest that the rhyolite magma at this locality probably rose as
a nearly vertical cylinder, as shown in figure 5B.

Most eruptions of rhyolite domes are preceded by pyroclastic explosions
in which pumice lapilli and ash form low cones around the vent (Williams,
1932). The subsequent eruption of viscous rhyolite magma produces the
rhyolite dome. Most domes form by internal expansion due to influx of
increasing amounts of viscous lava through the vent. In some domes, the outer
surface cools and hardens, then shatters, spilling loose fragments (crumble
breccia) down its sides. The dome continues to rise through a steep-sided
cone of crumble breccia. Except for the data from the drill hole, no data is
presently available to determine the geological relations at the base of the
domes; thus the relations shown in figure 5B are generalized, speculative, and
drawn largely from relations illustrated and described by Williams (1932) and
Macdonald (1972).

Petrology and chemistry

Rhyolite lavas exposed at East Butte are typically flow-banded and
consist of alternating layers of purple to gray rhyolite and glassy, tan,
devitrified rhyolite, each about 1 to 2 mm thick. Spherulites as much as
10 mm in diameter are present in the devitrified layers and, to a lesser

extent, in the glassy layers. Cleavage surfaces parallel to the flow-banding are typically grooved, furrowed, and corrugated, and contain sawtooth-like projections, all indicative of differential shear movement between the layers. In addition, the rock contains many small folds having wavelengths of several centimeters, which also point to the drag of adjacent layers. Locally, rhyolite lava flows on East Butte are more massive and lack conspicuous flow layering.

In thin section, the rhyolite of East Butte consists of phenocrysts of rounded and embayed sanidine (as much as 8 mm in diameter) and quartz (as much as 4 mm in diameter) set in a glassy, partly devitrified matrix. Rare phenocrysts of green diopsidic augite, fayalite, and plagioclase (An_{10}) are present. Rare micropegmatitic phenocrysts consist of sanidine and globular quartz. Quartz, tridymite, and potash feldspar in radiating patterns occur in spherulites. Grains and fine dusty particles of opaque minerals, reddish-oxidized biotite(?), zircon, apatite, and sphene are accessory minerals.

Rounded basalt inclusions as much as 15 cm in diameter are common in the rhyolite lavas of East Butte. The inclusions are porphyritic; plagioclase (An_{55}) laths as long as 25 mm are set in a reddish-oxidized matrix consisting of olivine, clinopyroxene, magnetite, plagioclase, and altered glass. The mineral assemblage and texture of the basalt inclusions are identical to those of basalt from a vent on the east side of East Butte (SW 1/4, sec. 13, T. 2 N., R. 32 E., fig. 4). We propose that the inclusions represent cinders or blocks of basalt lava that were incorporated into the rhyolite magma of East Butte as it rose through the same fissure system that localized the basalt vent, as discussed above. Spear (1979) suggests that the inclusions are hybrid in origin and were produced by the mechanical mixing of partly crystalline rhyolitic and basaltic magmas.

Rhyolitic breccias consisting of blocks of flow-banded rhyolite, pumice, and obsidian in a tuffaceous matrix are exposed on the surface of the unnamed dome. The mineralogy of the rhyolites of the unnamed dome is identical to that of the rhyolites of East Butte.

Available chemical analyses and normative compositions of rhyolite and a basalt inclusion from East Butte are given in table 5. The sum of the salic normative minerals (Q, Or, Ab, An) is greater than 95 percent, and the silica content is about 75 percent for the two rhyolite samples (analyses 1 and 2, table 5), indicating that they represent highly fractionated lavas. The analysis of the basalt inclusion from East Butte (analysis 3, table 5) shows that it is significantly different from other tholeiitic basalts of the ESRP (tables 2 and 3) and suggests contamination by the rhyolite magma.

Age and emplacement of the domes

Radiometric ages have been obtained for rhyolite from East Butte, the unnamed dome, the basalt that caps Middle Butte, and Big Southern Butte, a rhyolite dome located 20 km southwest of Middle Butte (table 6). These ages indicate that the rhyolite domes are relatively young and that their emplacement has occurred sporadically in time.

Volcanic domes occur chiefly in two geologic settings: as small (typically <4 sq km) protrusions in or near the summit craters of stratovolcanoes (Macdonald, 1972; Williams, 1932), and as late-stage intrusions and extrusive domes along ring fractures of large calderas (Smith and Bailey, 1968).

The rhyolite domes of this area clearly are more closely related to the second type than to the first. Previous workers have suggested that calderas are present at depth throughout the length of the ESRP but covered by a relatively thin veneer (1-2 km) of younger basalt lava flows (Armstrong and

Table 5.--Chemical analyses and CIPW normative minerals of two
rhyolites and one basalt inclusion from East Butte,
Eastern Snake River Plain, Idaho

		1	2	3
Location ------------		East Butte Rhyolite	East Butte Rhyolite	East Butte Basalt Inclusion
Field Sample No. ------		Unknown	MAK75-SEB1	72S51
USGS Lab. Sample No.		Unknown	W-192041	D103293
Collected by ------		Howard Powers	Mel A. Kuntz	George Stone
Chemical analysis				
	SiO_2	74.89	74.9	52.11
	TiO_2	.18	.13	2.28
	Al_2O_3	12.47	12.0	16.93
	Fe_2O_3	2.11	1.0	3.55
	FeO	.20	1.2	7.48
	MnO	.05	.04	.22
	MgO	.07	.02	2.55
	CaO	.59	.61	7.40
	Na_2O	3.84	3.9	4.16
	K_2O	5.13	5.0	1.71
	P_2O_5	.02	—	1.14
	H_2O+	.01	.60	.18
	H_2O-	.05	.13	.04
	CO_2	.01	—	.02
	Total	99.62	99.5	99.77
CIPW normative minerals				
	Q	32.01	31.92	3.04
	Or	30.45	29.73	10.13
	Ab	32.63	33.20	35.30
	An	1.65	.47	22.53
	Di:	.38	2.28	5.56
	Wo	.20	1.07	2.79
	En	.18	.05	1.28
	Fs	—	1.16	1.49
	Hy:	—	.09	11.07
	En	—	—	5.09
	Fs	—	.09	5.97
	MT	.29	1.46	—
	Hm	1.92	—	—
	Il	.34	0.25	—
	Ap	.05	—	—
	Cc	.02	—	—

Table 6.--Potassium-argon ages of rhyolite domes along the axis of the
central part of the eastern Snake River Plain, Idaho

Rhyolite dome	Age	Reference
East Butte--------	0.58±0.09 m.y.	Armstrong and others, 1975.
Middle Butte------	Rhyolite not exposed; basalt flow capping butte is 1.9±1.2 m.y.	Armstrong and others, 1975.
Unnamed dome between Middle Butte and East Butte.	1.42±0.02 m.y.	G. Brent Dalrymple, USGS, unpublished data, 1978.
Big Southern Butte	0.304±0.022 m.y.	G. Brent Dalrymple, USGS, unpublished data, 1977; Kuntz, 1978b, 1978c

others, 1975; Eaton and others, 1975; Christiansen and McKee, 1978). Such an idea is now supported by accumulating field evidence on the distribution and age of rhyolite ash flows around the margins of the ESRP. Drilling data (Doherty and others, 1979) from a 3,159 m (10,365 ft) geothermal exploration well (INEL-1) drilled on the INEL (fig. 2) about 22 km northwest of Middle Butte suggest that a caldera is present. The upper part of the well passed through 744 m (2,440 ft) of basalt lava flows and interbedded sediments. Sedimentary interbeds in the upper part of the basalt section are thin (<30 m) and of alluvial and lacustrine origin, those in the lower part are thicker (45 to 100 m) and dominantly tuffaceous. The depth interval between 744 m (2,440 ft) and 2,460 m (8,070 ft) consists of welded ash flow tuffs, as thick as 425 m (1,400 ft) and averaging about 90 m (300 ft), interbedded with airfall ash deposits, tuffaceous sediments, and nonwelded airfall ash flows. The lower 745 m (2,445 ft) penetrated by the well consists of dense, highly altered rhyodacite ash flows(?) of uniform texture.

These observations suggest that the ash flows represent a thick accumulation of volcanic ejecta within an already formed caldera depression or filling that was concurrent with caldera collapse. The data support the idea that calderas and related rhyolitic ash flows are present beneath the cover of basalt lavas in the ESRP. Drilling and geophysical data are not sufficient to define the ring-fracture system of the inferred caldera with precision, but subtle topographic and drainage features and the distribution of the rhyolite domes, basalt volcanoes, and volcanic rift zones suggest a general location for the ring fracture as shown in figure 2.

Magnetotelluric soundings (Stanley and others, 1977) and unpublished Curie isotherm maps by the late Bimal Bhattacharyya of the U.S. Geological Survey (Don Mabey, USGS, oral commun., 1979) for the ESRP indicate that a

ridge of high temperature exists at shallow depth beneath the plain in the vicinity of the rhyolite domes. Sufficient heat may still be present in the deep crust to resupply rhyolitic magma to the caldera at periodic intervals, and the intrusion of the domes is controlled by ring fractures along the southern margin of the caldera. Once rhyolite magma reaches the basalt-rhyolite interface above the caldera ring fracture, its emplacement at the surface is augmented by the density contrast between dense basalt and lighter rhyolite magma.

One argument against the notion that the domes are post-collapse intrusions along a caldera ring fracture involves the timing of such intrusions in other well-studied calderas. Smith and Bailey (1968) have noted that domes are emplaced along ring fractures approximately 100,000 to 1 m.y. after caldera collapse. The age of the inferred caldera penetrated by the geothermal exploration well is not known with certainty, but an age of 5-10 m.y. seems reasonable on the basis of known ages and stratigraphic relations of ash flows along the margins of the ESRP (Armstrong and others, 1975; Prostka and Embree, 1978). The ages of the three rhyolite domes are thus too young by approximately 4 to 10 million years to satisfy the caldera model of Smith and Bailey.

A similar and equally plausible explanation for the origin and emplacement of the domes is that they represent remelted and remobilized rhyolitic rocks that were related to an older caldera cycle (Schoen, 1974). The high crustal temperature at shallow depth in the vicinity of the rhyolite domes, as described above, indicates that melting of lower and middle crustal rocks is a likely contemporaneous process. Structural control of the emplacement of the domes could thus be related to volcanic rift zones, preexisting vents for basalt volcanoes or other structures. Additional

drilling and geophysical data will likely lend support to one or the other of the ideas presented here or perhaps to different ideas.

Regardless of the mode of origin of the domes, it seems clear that they were emplaced at the surface as a result of relatively unexplosive eruptions, as is evident from their field relations. This type of eruption may have been caused by the loss of gases from the magma to the water-saturated or otherwise porous basalt-sediment lid through which the domes protruded before reaching the surface. Future eruptions of rhyolite domes near Middle and East Buttes would likely be of similar character.

K-AR AGES OF BASALT LAVA FLOWS IN CORED DRILL HOLES

AT THE PROPOSED STF REACTOR SITE

Analytical Technique

Thin sections of 87 samples from five cores at the proposed STF reactor site were examined using a petrographic microscope to determine those most suitable for K-Ar dating. Twenty-nine of the thin sections were selected for more detailed petrographic study and, 15 rock samples from flow units I through VB were chosen for K-Ar analysis, including 4 from hole CH-C7, 3 from hole CH-E7.90, 1 from hole CH-G.4-8.05, 4 from hole CH-11.25, and 3 from hole CH-G12 (see Kuntz, 1978a). In general, the samples analyzed meet the criteria of acceptability for whole-rock K-Ar dating (Mankinen and Dalrymple, 1972), in that they are unaltered. Nine of the samples, however, contain from 3 to 10 percent of fresh, brown to pale-brown glass in the groundmass; the remaining 6 samples contain a trace (<1 percent) of glass in the groundmass. Because of the age and K_2O contents of these basalts, however, the presence of glass should have little or no effect on the calculated K-Ar ages; and any errors due to Ar loss from the glass should be well within the analytical uncertainties.

The samples for analysis were crushed using a jaw crusher and a hardened steel roller mill, then sieved with stainless steel sieves to a size of 1-2 mm. An aliquot of this sized material was pulverized to a very fine powder with a Shatterbox pulverizer, using hardened steel crucibles and pucks, and measured for K_2O content. Aliquots of the remaining sized material were used for the Ar analyses.

Potash was measured by flame photometry using the lithium metaborate fusion technique (Ingamells, 1970) and appropriate standards. The quantity of ^{40}K was calculated from the K_2O results using an abundance of 1.167×10^{-4} mole ^{40}K/mole K (Garner and others, 1975). Four independent K_2O analyses were made on each of the 15 samples dated.

Radiogenic ^{40}Ar was measured by isotope-dilution mass spectrometry using techniques described by Dalrymple and Lanphere (1969). Except for sample MAK77-S114, two independent aliquots of each sample were extracted and measured (table 7, extraction nos. 1, 2, and so forth. The samples, which ranged in weight from 12 to 27 g, were placed in pre-fired molybdenum crucibles and baked overnight in ultra-high vacuum extraction lines at $280^{\circ}C$. Fusion was by induction heating using a 7.5-kw induction generator. During fusion, a ^{38}Ar tracer was introduced. Reactive gases, including H_2, O_2, and CO_2, were removed by reaction with hot CuO and hot Ti metal; H_2O was removed by adsorption with a 5 Å artificial zeolite molecular sieve. The Ar was collected in breakseal tubes by adsorption on activated charcoal cooled by LN_2 for mass spectrometric analysis.

Three separate ^{38}Ar tracer systems (K, M, and N) were used in the measurements, as indicated in table 7. All are bulb tracers and contain high-purity ^{38}Ar (>>99 percent). Their ^{38}Ar concentrations are traceable, through standards, to absolute-air Ar calibration, and their calibrations are frequently checked with intralaboratory standards. Interlaboratory

Table 7.--Potassium-argon age data for samples of basalt from drill holes at the STF site, ANLW-INEL, Idaho

							Argon				A	B
Flow	Sample No.	K_2O^a (wt pct)	Extrac-tion	Weight (g)	Tracer	Mass analysis No.	$^{40}Ar/^{38}Ar$	$^{38}Ar/^{36}Ar$	$^{40}Ar_{rad}$ (mol/g)	$^{40}Ar_{rad}$ (percent)	Calculated age[b] (10^3 years)	Weighted mean[c] (10^3 years)
I	MAK77-S47	0.553±0.014	1	25.387	N	A	2.1759	133.82	Nil	Nil	<490	
												<450
			2	25.356	N	A	1.9644	148.82	--do--	--do--	<450	
	MAK77-S66	0.544±0.002	1	25.504	N	A	2.5018	116.64	--do--	--do--	<570	
												<490
			2	26.212	N	A	2.1904	133.39	--do--	--do--	<490	
	MAK77-S119	0.540±0.001	1	25.449	N	A	2.0986	139.38	--do--	--do--	<490	
												<490
			2	25.749	N	A	2.6904	108.68	--do--	--do--	<620	
II	MAK77-S50	0.604±0.007	1	24.974	M	A	4.7925	62.850				
									$5.648±10^{-13}$	2.0	650±130	
						B	4.7900	62.726				
												530±90
			2	25.689	M	A	4.3681	68.518				
									3.742	1.5	430±120	
						B	4.3677	68.507				
	MAK77-S86	0.616±0.006	1	15.397	M	A	2.0908	142.94				
									3.190	1.6	360±95	
						B	2.0917	142.93				
												320±65
			2	22.077	M	A	2.7760	107.56	2.541	1.4	285±85	
	MAK77-S122	0.602±0.002	1	25.049	M	A	3.1742	95.216				
									4.462	2.3	515±85	
						B	3.1715	94.981				
												405±60
			3	24.726	M	A	3.0930	96.711				
									2.561	1.4	295±85	
						B	3.0881	96.577				

43

Flow	Sample No.	K_2O^a (wt pct)	Extraction	Weight (g)	Tracer	Mass analysis No.	$^{40}Ar/^{38}Ar$	$^{38}Ar/^{36}Ar$	$^{40}Ar_{rad}$ (mol/g)	$^{40}Ar_{rad}$ (percent)	A Calculated age[b] (10^3 years)	B Weighted mean[c] (10^3 years)
III	MAK77-S54	0.588±0.002	1	25.518	M	A	4.5993	65.244				
									4.244	1.6	500±130	
						B	4.5915	65.145				
												460±85
			2	25.007	M	A	3.9041	76.666				
						B	3.9032	76.825	3.643	1.5	430±110	
						C	3.8990	76.728				
	MAK77-S72	0.558±0.001	1	26.298	K	A	8.6758	34.538				
									3.724	1.4	450±130	
						B	8.6683	34.529				
												395±85
			2	26.902	K	A	7.2552	41.272				
									2.952	1.4	360±105	
						B	7.2560	41.236				
	MAK77-S107	0.586±0.001	1	25.187	M	A	1.6808	178.74				
									2.155	2.1	255±55	
						B	1.6793	178.78				
												270±40
			2	25.193	M	A	2.0691	145.20				
									2.400	1.9	285±60	
						B	2.0685	144.82				
	MAK77-S108	0.585±0.001	2^d	27.095	K	A	7.5247	40.116				
									4.253	1.9	530±105	
						B	7.5091	39.961				
												390±60
			4^d	12.144	M	A	1.4109	211.60				
									3.004	1.8	360±50	
						B	1.4102	212.08				

44

Flow	Sample No.	K_2O[a] (wt pct)	Extraction	Weight (g)	Tracer	Mass analysis No.	$^{40}Ar/^{36}Ar$	$^{38}Ar/^{36}Ar$	$^{40}Ar_{rad}$ (mol/g)	$^{40}Ar_{rad}$ (percent)	A Calculated age[b] (10^3 years)	B Weighted mean[c] (10^3 years)
IV	MAK77-S111	0.742±0.005	1	26.916	K	A	13.633	21.953	5.378	1.3	505±150	
												440±85
			2	26.521	K	A	6.1583	49.139				
									4.563	2.5	425±70	
						B	6.1628	49.091				
	MAK77-S129	0.809±0.004	1	25.904	M	A	1.9746	153.83				
									3.699	3.2	320±40	
						B	1.9721	154.11				
												310±30
			2	25.258	M	A	2.0850	144.87				
									3.502	2.8	300±45	
						B	2.0864	145.34				

Flow	Sample No.	K_2O[a] (wt pct)	Extraction	Weight (g)	Tracer	Mass analysis No.	Argon $^{40}Ar/^{38}Ar$	$^{38}Ar/^{36}Ar$	$^{40}Ar_{rad}$ (mol/g)	$^{40}Ar_{rad}$ (percent)	A Calculated age[b] (10^3 years)	B Weighted mean[c] (10^3 years)
VA	MAK77-S114	0.944±0.010	1[e]	25.679	M	A	2.9311	104.29	6.076	3.4	450±50	450±50
						B	2.9306	103.84				
	MAK77-S78	0.942±0.008	1	25.933	K	A	9.3363	32.570				
									8.003	2.8	590±80	
						B	9.3173	32.538				
												595±60
			2	26.081	K	A	10.126	29.943	8.181	2.6	605±90	
VB	MAK77-S63	0.998±0.002	1	21.632	K	A	5.0692	60.456				
						B	5.0693	60.366	6.451	3.4	450±50	
						C	5.0647	60.030				
												460±40
			2	25.330	K	A	6.8806	44.250				
									6.711	3.1	470±60	
						B	6.8823	44.248				

[a] Mean and standard deviation of four measurements.

[b] $\lambda_\epsilon + \lambda_\epsilon' 0.581 \times 10^{-10}$ yr^{-1}, $\lambda_\beta = 4.962 \times 10^{-10}$ yr^{-1}, $^{40}K/K = 1.167 \times 10^{-4}$ mol/mol. Errors are estimates of the standard deviation of precision (Cox and Dalrymple, 1967).

[c] Weighting is by the inverse of the variance.

[d] Samples 1 and 3 were lost because of technical difficulties.

[e] Sample 2 was lost because of technical difficulties.

Note: The ages listed here differ significantly from ages published earlier (Kuntz, 1978a). The original ages were calculated using a defective computer program and the correct ages are listed here.

comparisons of the U.S. Geological Survey, Menlo Park laboratory, with other geochronological laboratories throughout the world can be found in Lanphere and Dalrymple (1976). Uncertainties in the composition and absolute concentrations of the Ar isotopes and in the bulb-depletion constants contribute negligible errors to the Ar analyses in this study.

The mass spectrometric analyses of samples from flows II-VA were done in the static mode using a multiple collector, first-order, direction-focusing mass spectrometer designed and constructed by the U.S. Geological Survey. The analyzer has a radius of 22.86 cm and a nominal magnet sector of 90°. The instrument has a more-or-less conventional gas ion source that operates at an accelerating voltage of 2 kilovolts. The collector assembly contains five independent faraday cup ion collectors appropriately spaced for the isotopes ^{36}Ar through ^{40}Ar and alined on the focal plane. Each ion collector has its own independent data channel consisting of an electrometer, A-D converter, optical isolater, and 23-bit digital counter. The mass spectrometer operates under control of a dedicated PDP8/e minicomputer, which controls the magnetic field and takes data from the data channels and the internal elapsed time clock. Because the instrument utilizes a separate collector for each isotope, all data channels can be controlled and read by the computer simultaneously and at high speed. Magnet switching is required only for baseline measurements. This approach virtually eliminates problems caused by the memory effect in conventional Ar mass spectrometers and results in a significant increase in precision. This study probably would not have been successful without this unique instrument. This instrument and its operating characteristics are described in detail by Stacey and others (1978) and by Sherrill and Dalrymple (in press).

47

The mass spectrometric analyses of samples for flow I were done using a single-collector, first-order, direction-focusing mass spectrometer that utilizes on-line data acquisition and computer-controlled magnetic-field switching. The quality of the data acquired using this instrument is similar to that obtained using the five-collector instrument.

With only a few exceptions, the isotopic composition of the gas from each Ar extraction was measured more than once on successive aliquots (or splits) (table 7, mass spectrometer run A, B, and so forth); and the mean of the resulting Ar ratios, after appropriate corrections for mass discrimination, was used to determine the quantity of radiogenic ^{40}Ar. Each individual analysis on the five-collector instrument is based on 150 values from each of three data channels (^{36}Ar, ^{38}Ar, and ^{40}Ar) using a one-second integration time and taken over a 2.5-minute period. Baseline and background data for each channel are in addition to the 150 peak readings. The single-collector instrument acquires nine readings on each of the three mass peaks during a 15-minute period, in addition to the appropriate background and baseline readings. Instrumental discrimination for both spectometers was measured using atmospheric Ar and was ≤0.25 percent/mass unit during the course of this study. Slightly more than half of the duplicate measurements on the same sample gas agreed to within 0.1 percent (that is, ± 0.05 percent), and the worst replication observed was 0.56 percent (± 0.28 percent) (fig. 6).

Ages were calculated using the new ^{40}K decay ($\lambda_\varepsilon + \lambda_\varepsilon' = 0.581$ x 10^{-10} yr^{-1}, $\lambda_\beta = 4.962$ x 10^{-10} yr^{-1}) and abundance (^{40}K/K=1.167 x 10^{-4} mol/mol) constants recommended by the IUG Subcommission on Geochronology (Steiger and Jäger, 1977).

Results

The K_2O measurements on individual samples (table 3) are consistent with the petrographic correlations of flows between cores (Kuntz, 1978a), showing

Figure 6.--Cumulative curve showing percent difference (Δ) between 41

duplicate Ar ratios measured for 23 samples of basalt from cores at the

STF site Argonne National Laboratory-West, Idaho National Engineering
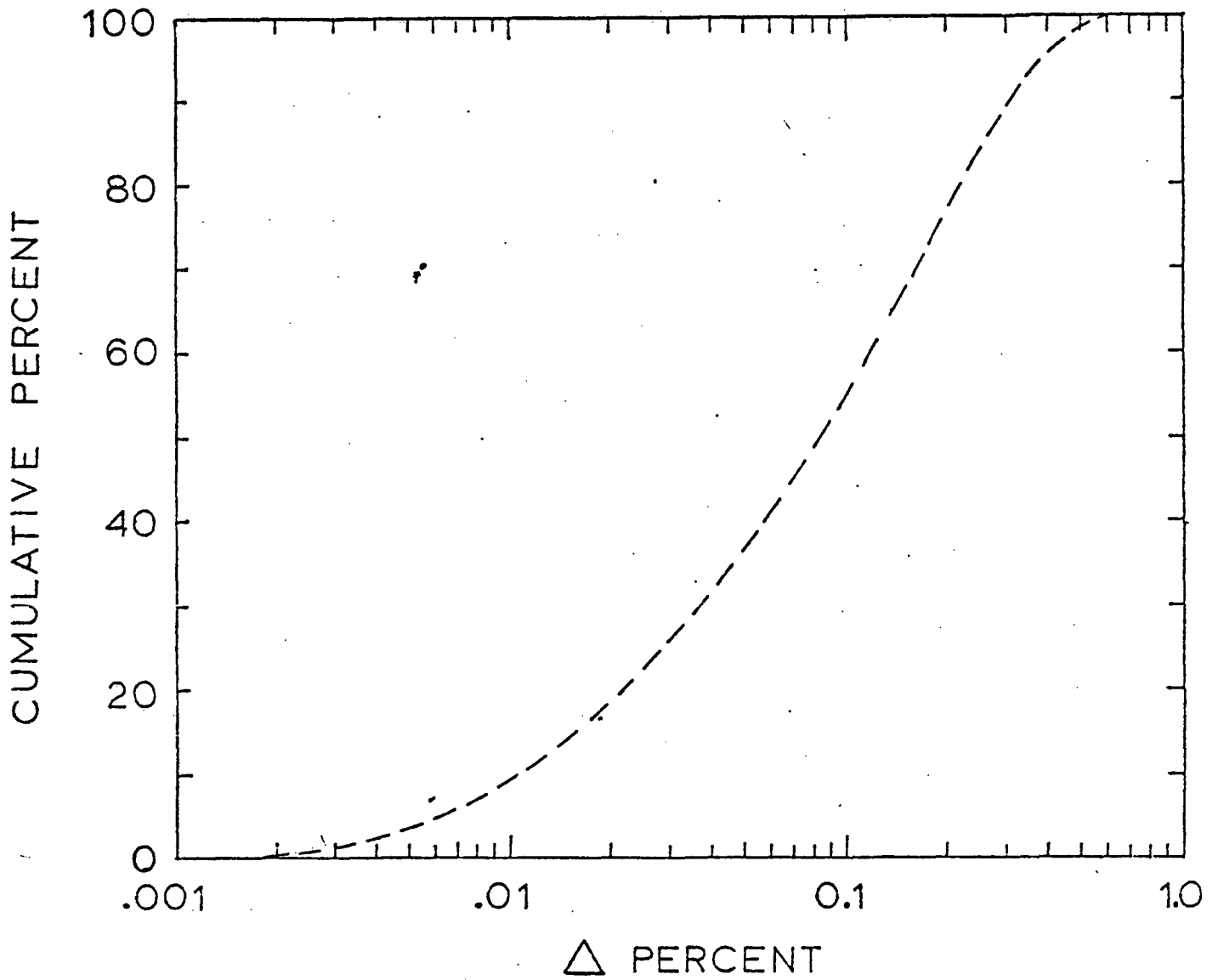
Laboratory, Idaho.

Figure 6.—Cumulative curve showing percent difference (Δ) between 41
duplicate Ar ratios measured for 23 samples of basalt from cores at the
STF site, Argonne National Laboratory–West, Idaho National Engineering
Laboratory, Idaho.

no more variation within the individual flows than was expected from previous studies (Dalrymple and Hirooka, 1965).

The analytical data, the calculated K-Ar ages, and the weighted mean ages of duplicate argon extractions are given in table 7. Because the six flows analyzed are both geologically very young and low in potassium, the amount of radiogenic ^{40}Ar relative to atmospheric ^{40}Ar in the sample gas is small, ranging from 0 to only 3.4 percent. As a result there is considerable scatter in the results and the estimated errors in the calculated ages for individual samples are large, ranging from 11 to 30 percent. The reason is that the theoretical error in a K-Ar age increases rapidly as the percentage of radiogenic ^{40}Ar decreases below about 10 percent (fig. 7). The error calculations are also very sensitive to the estimates of the errors in the individual quantities measured. For example, for a sample with 2 percent radiogenic ^{40}Ar, an increase in the estimated error of the ^{38}Ar/^{36}Ar ratio from 0.5 to 1.0 percent nearly doubles the theoretical error in the calculated age. Finally, the error calculations do not take into account geological factors, such as sample inhomogeneity, that frequently result in larger errors than the measurements. Because of these factors, errors assigned to the calculated ages are only estimates of analytical precision for single samples. and the data should be treated accordingly.

The data for each flow unit have been treated statistically in several ways, as summarized in table 8. Column 1 of this table gives the simple means and calculated standard deviations of all of the calculated ages for each flow in column A of table 7. Column 2 gives the means and standard deviations of the data in column B of table 7. Neither of these methods, however, takes into account the estimated errors in analytical precision for each calculated age, so a poor analysis is given the same weight as a better analysis. Column 3 contains the weighted means, where weighting is by the inverse of the

Figure 7.--Theoretical error curve for K-Ar ages as a function of the
percentage of radiogenic ^{40}Ar in the sample gas. Based on the error
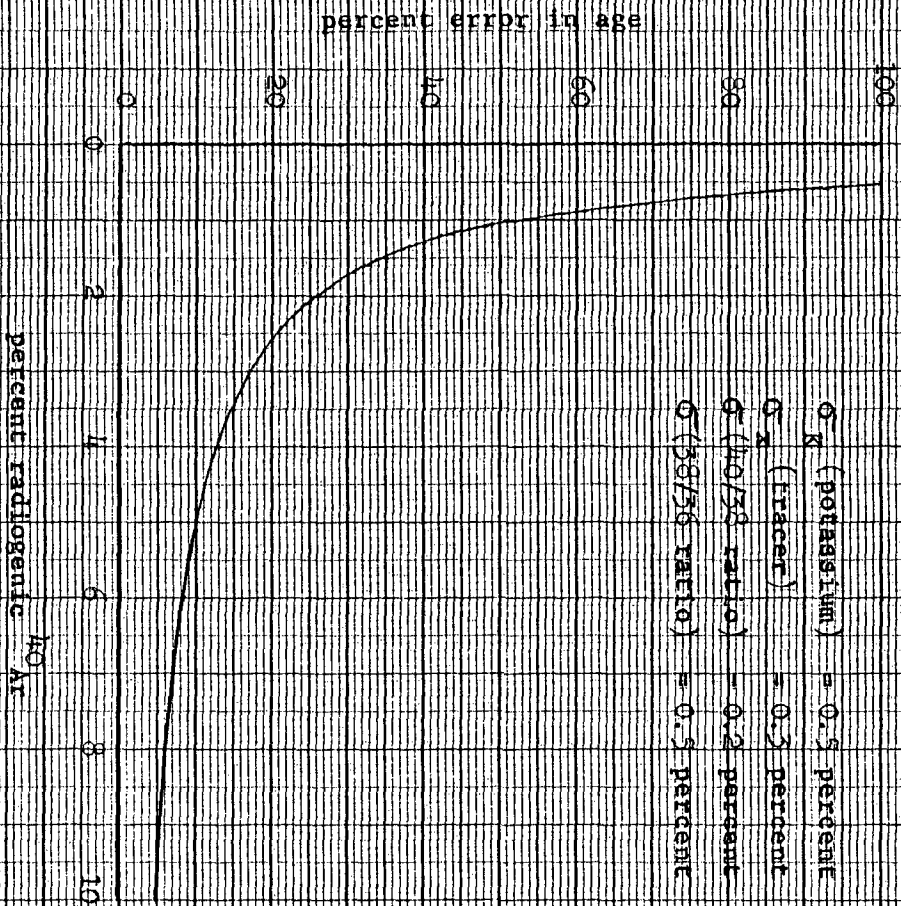formula of Cox and Dalrymple (1967).

K+E 10 X 10 TO THE CENTIMETER 18 X 25 CM.
KEUFFEL & ESSER CO. MADE IN U.S.A.

461510

percent error in age

percent radiogenic ^{40}Ar

σ_K (potassium) = 0.5 percent
σ_x (tracer) = 0.3 percent
σ (40/38 ratio) = 0.2 percent
σ (38/36 ratio) = 0.5 percent

Fig. 7. Theoretical error curve for K-Ar ages as a function of the percentage of radiogenic ^{40}Ar in the sample gas. Based on the error formula of Cox and Dalrymple (1967).

Table 8.—Mean flow ages for data in table 7

Flow	Mean age (10^3 years) [1] 1	2	3	Probability of difference in calculated ages of column 3	Δ [2] (10^3 years)
I	<450	<450	<450		
					(0-400)
II	420±140	420±105	400±40		
				.78	0 (0-100)
III	395±100	380±80	335±35	.79	
				.13 .95	0 (0-100)
IV	385±95	375±90	325±45	1.0 .71	
				1.0 .98	185 (100-250)
VA	550±85	520±100	510±40	.98	
				.62	0 (0-100)
VB	460±15	–	460±40		

[1] Method:
1—Simple mean and standard deviation of calculated ages in column A, table 7.
2—Simple mean and standard deviation of calculated ages in column B, table 7.
3—Weighted mean of calculated ages in column B, table 7. Estimated uncertainties are at the 68 percent confidence level.

[2] Apparent difference in age of adjacent flows (Δ) and estimated range of Δ.

Note: The ages listed here differ significantly from ages published earlier (Kuntz, 1978a). The original ages were calculated using a defective computer program and the correct ages are listed here.

variance of the mean ages for each sample (column B, table 7). This technique takes into account the estimated analytical uncertainties of the individual measurements as well as the number of measurements made on each sample. The mean ages in column 3 are probably the least biased. An important result of the means in table 7 is that the resulting mean age of each flow unit is relatively independent of the way in which the data are treated, especially when the uncertainties of the data are considered.

We have calculated the probability of a detectable age difference between flows based on the weighted mean ages and uncertainties given in column 3, table 7. We would like to emphasize that the uncertainties in the flow ages are poorly known and the probabilities are, therefore, only rough estimates. The last column in table 8 is the apparent differences in age between superposed flows and an estimate of the range of possible age differences. Apparent age differences that are contrary to the known stratigraphic order are assigned a value of zero.

Radiogenic ^{40}Ar was not detected in any of the samples from flow I. The maximum ages in tables 6 and 7 were calculated on the assumption that 2 percent radiogenic ^{40}Ar would have been detected if present. The time interval between the eruption of flows I and II is not known, but it could have been as much as $300\text{--}400 \times 10^3$ years or as little as perhaps 1×10^3 years. No difference was detected in the apparent ages of flows II-IV at the 80 percent level of confidence. The times between eruption of flows II and III or III and IV could be as little as perhaps 1×10^3 years and as much as perhaps 100×10^3 years. It is unlikely, however, that flows II-IV represent more than about 150×10^3 years. No difference was detected in the ages of the lowermost two flows, VA and VB, and both are approximately 500×10^3 years

old. It appears that as little as 100 x 10³ years or as much as 250 x 10³ years may have passed between the eruption of flows IV and VA.

A rough estimate of the time span between successive flows can be estimated from the amount of loess that occurs between the base of an overlying flow and the top of an underlying flow. It seems logical that loess accumulation in the eastern Snake River Plain has not been uniform throughout the Pleistocene, but we conclude that a greater thickness of loess between flows implies a greater time interval between the time of emplacement of the underlying and overlying flows.

Data presented by Kuntz (1978a) show that as much as about 3 m (10 ft) of loess occurs on top of flow I, as much as about 2 m (6 ft) on top of flow IV, and as much as about 0.6 m (2 ft) on top of flow VA. All other flows are covered by less than about 0.3 m (1 ft) of loess. These data suggest that flow I is probably relatively old, possibly on the order of 100-300 x 10³ years, and that the time span between the emplacement of flows I and II and flows II and III was short, possibly on the order of 1 x 10³ to as much as 100 x 10³ years. The relatively thick accumulation of loess resting on flow IV suggests that the time span between the emplacement of flows III and IV was long, possibly as much as 100 x 10³ years. The thickness of loess between flows IV and VA and flows VA and VB suggests that the time intervals between these flows were short, possibly as little as 1 x 10³ years.

The data discussed above and the age data in tables 7 and 8 lead to the tentative conclusions that flow I was erupted between 100 x 10³ and 300 x 10³ years ago, that flows II and III were erupted approximately 350 x 10³ years ago, that flow IV occurred about 400 x 10³ years ago, and that flows VA and VB were erupted about 450 x 10³ to 500 x 10³ years ago.

POTENTIAL VOLCANIC HAZARDS

Volcanic hazards for the STF and ANLW facilities are governed chiefly by three factors: (1) topography, (2) location of volcanic vents, and (3) recurrence interval of volcanism that produced lava flows which traversed the site of the ANLW facility.

Topographic Factors

The ANLW facility lies in a U-shaped topographic depression, here called an "eruption basin," which is bounded on the northeast and east by volcanoes of the Lava Ridge-Hells Half Acre volcanic rift zone and on the south and southwest by volcanoes and rhyolite domes located along the long axis-topographic ridge of the ESRP near East Butte (figs. 3 and 8; Kuntz and others, 1979). Future volcanic activity near the ANLW facility is likely to be localized along these two topographic highs. Thus, future volcanoes have the potential of delivering lava flows into the "eruption basin" and to the site of the ANLW facility.

Location and Type of Future Volcanic Vents

Figure 8 shows the location of possible future volcanic vents (zone 1) that would pose the most threat to the ANLW facility. Zone 1 includes all of the area lying between the topographic ridges bounding the "eruption-hazard basin," and the area lying east, north, and west of the facility that lies above the 1,555 m (5,100 ft) elevation. (Elevation of ANLW facility is about 1,569 m (5,150 ft). Lavas erupted from future volcanic vents in zone 2 (fig. 8) would likely pose less of a volcanic hazard because (1) such lavas would have to flow across the topographic ridges bounding the "eruption basin" to reach the facility, and (2) future volcanic vents in zone 2 to the north of the facility would have to build volcanic cones that reach an elevation greater than the elevation of the facility.

Figure 8.--Generalized map showing geology, topography, and volcanic hazard zones in the vicinity of the ANLW facilities, INEL, Idaho. Geology and topography simplified from Kuntz and others, 1979.

EXPLANATION

▓▓▓ Volcanic hazard zone 1

·:·:· Volcanic hazard zone 2

Topographic divide

Contour (elev. in ft.)

Contact, "Y" and "O" refer to younger and older flows

⊙ X Volcanic vents, large and small

Flow direction

Lava channel

0 1 2 3 4 5
Kilometers
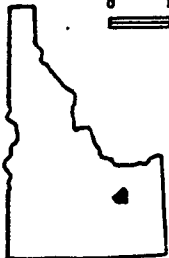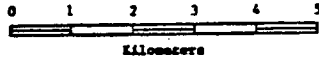
State of Idaho showing
location of area shown
in figure
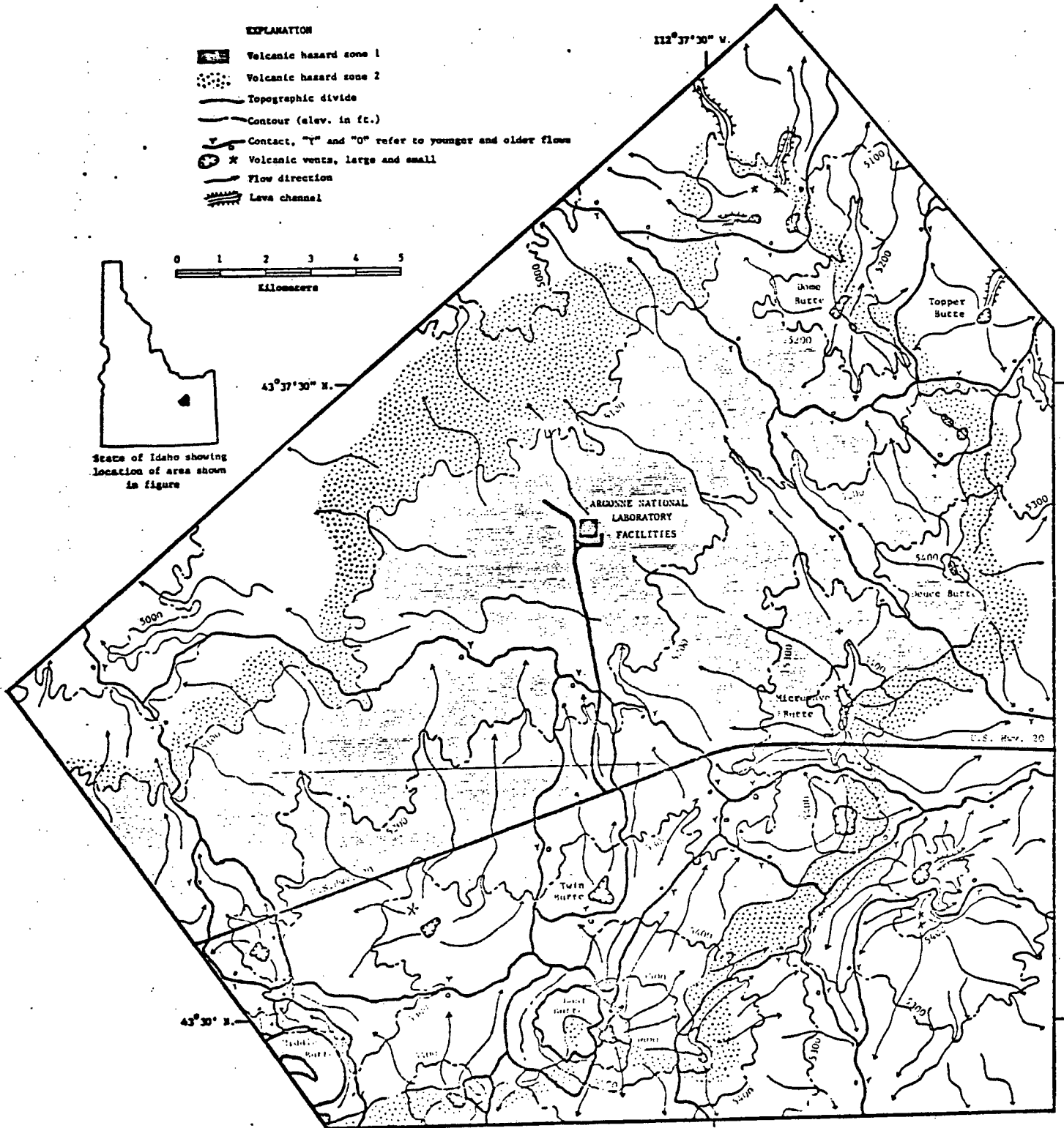
Inasmuch as most of the volcanoes in volcanic hazard zones 1 and 2 are of the lava-cone and shield-volcano types, it is reasonable to assume that future basalt volcanism will also be of this type and produce similar vent structures and corresponding lava flows. Thus the type of volcanic hazard most likely to occur at the ANLW facility would involve flooding by lava flows from shield volcanoes located chiefly in zone 1 and, less likely, in zone 2 of figure 8.

As shown in figure 2, few basalt volcanoes are located within the ring-fracture zone of the inferred rhyolite caldera, suggesting that the deep crust there is still too hot to deform by regional deviatoric stresses. As a result, basalt magma is less likely to be erupted within the ring-fracture zone. Facilities of the ANLW are located approximately 5 km from the ring fracture zone; thus the likelihood of the future eruption of a basalt volcano within the facilities seems remote.

The eruption of future rhyolite domes in the Lava Ridge-Hells Half Acre area will likely occur along the topographic ridge near Middle Butte and East Butte (figs. 3 and 8), more than 12 km south of the ANLW facility. The rhyolite domes at this locality were probably erupted by the nonexplosive protrusion of viscous rhyolite magma. However, eruption of some rhyolite domes is explosive, associated with pyroclastic flows and air-fall tephra. Collapse of rhyolite domes may produce block flows and ash flows capable of moving several kilometers down steep slopes. A rhyolite-dome eruption in the vicinity of Middle Butte and East Butte would constitute a volcanic hazard for the ANLW facility if it were of the explosive variety, produced tephra that could be carried by winds to the facility, and produced large volumes of block or ash flows.

In light of the nonexplosive nature of past rhyolite eruptions, it seems reasonable to conclude that future rhyolite eruptions would also be of this nature and pose little volcanic hazard to the ANLW facility.

It is unreasonable to assume that reactivation of the inferred rhyolite caldera (fig. 2) in the form of collapse and generation of a major ash-flow sheet will occur in the future. (See Smith and Bailey, 1968.) Possible future ash-flow eruptions related to collapse of rhyolite calderas in the Yellowstone region would be unlikely to affect the ANLW facilities.

Volcanic Recurrence Intervals

The average recurrence interval of basalt lava flows sampled in the drill holes is $80-100 \times 10^3$ years. It is clear from the K-Ar data, however, that the flows were erupted at irregular intervals and that volcanism has not been periodic. Times between successive flows may be as short as $1-10 \times 10^3$ years and as long as $300-400 \times 10^3$ years. Although it is not possible to predict when the next lava flow might occur, it may be useful to compare these findings with one of the criteria used by the U.S. Nuclear Regulatory Commission (10CFR100, Appendix A, paragraph III(g)) and adopted by ANS 2.7 (Guidelines For Assessing Capability For Surface Faulting At Nuclear Power Reactor Sites) to define a capable fault for the purposes of Nuclear Power Reactor siting evaluation:

> "Movement at or near the ground surface at least once within the past 35,000 years or movement of a recurring nature within the past 500,000 years."

The K-Ar data definitely show that at least five episodes of volcanic activity have resulted in the inundation of the ANLW facilities site by basalt lava flows within the past 500,000 years.

Summary

We judge that the chief potential volcanic hazard for the ANLW facilities involves inundation by basalt lava flows erupted from volcanic vents lying in volcanic hazard zone 1 (fig. 8). Future eruptions in volcanic hazard zones 1 and 2 may occur more frequently than once in approximately every $80-100 \times 10^3$ years, but the likelihood that a given eruption will produce lava flows that cover the facility is approximately once in every $80-100 \times 10^3$ years.

REFERENCES CITED

Armstrong, R. L., Leeman, W. P., and Malde, H. E., 1975, K-Ar dating of
Quaternary and Neogene volcanic rocks of the Snake River Plain, Idaho:
American Journal of Science, v. 275, p. 225-251.

Beutner, E. C., 1968, Structure and tectonics of the southern Lemhi Range,
Idaho: The Pennsylvania State University Ph.D. thesis, 181 p.

Braile, L. W., 1978, Seismic and gravity models of the Snake River Plain, in
1978 International Symposium on the Rio Grande Rift, Program and
Abstracts: Los Alamos Scientific Laboratory, N. M., Document LA-7487-C,
p. 19.

Christiansen, R. L., and McKee, E. H., 1978, Late Cenozoic volcanic and
tectonic evolution of the Great Basin and Columbia intermontane regions,
in Smith, R. B., and Eaton, G. P., eds., Cenozoic tectonics and regional
geophysics of the Western Cordillera: Geological Society of America
Memoir 152, p. 283-312.

Cox, A., and Dalrymple, G. B., 1967, Statistical analysis of geomagnetic
reversal data and the precision of potassium-argon dating: Journal of
Geophysical Research, v. 72, p. 2603-2614.

Dalrymple, G. B., and Hirooka, K., 1965, Variation of potassium, argon, and
calculated age in a late Cenozoic basalt: Journal of Geophysical
Research, v. 70, p. 5291-5296.

Dalrymple, G. B., and Lanphere, M. A., 1969, Potassium-argon dating: San
Francisco, W. H. Freeman and Company, 258 p.

Doherty, D. J., 1979, Drilling data from exploration hole 1, NE 1/4, sec. 22,
T. 2 N., R. 32 E., Bingham County, Idaho: U.S. Geological Survey Open-
File Report 79-1225, 1 p.

Doherty, D. J., McBroome, L. A., and Kuntz, M. A., 1979, Preliminary
geological interpretation and lithologic log of the geothermal
exploration well (INEL-1), Idaho National Engineering Laboratory, eastern
Snake River Plain, Idaho: U.S. Geological Survey Open-File Report
79-1248, 7 p.

Eaton, G. P., Christiansen, R. L., Iyer, H. M., Pitt, A. M., Mabey, D. R.,
Blank, H. R., Zietz, I., and Gettings, M. E., 1975, Magma beneath
Yellowstone National Park: Science, v. 188, p. 787-796.

Fabbi, B. P., and Espos, L. F., 1976, X-ray fluorescence analysis of 21
selected major, minor, and trace elements in eight new USGS standard
rocks: U.S. Geological Survey Professional Paper 840, p. 89-93.

Garner, E. L., Murphy, T. J., Gramlich, J. W., Paulsen, P. J., and Barnes, I.
L., 1975, Absolute isotopic abundance ratios and the atomic weight of a
reference sample of potassium: National Bureau of Standards Journal of
Research, A, Physics and Chemistry, v. 79A, p. 713-725.

Gary, M., McAfee, R., Jr., and Woff, C. L., eds., 1972, Glossary of Geology:
Washington D.C., American Geological Institute, 805 p.

Hait, M. H., Jr., and Scott, W. E., 1978, Holocene faulting, Lost River Range,
Idaho: Geological Society of America Abstracts with Programs, v. 10,
no. 5, p. 217.

Hill, D. P., and Pakiser, L. C., 1967, Seismic-refraction of crustal structure
between the Nevada Test Site and Boise, Idaho: Geological Society of
America Bulletin, v. 78, p. 685-704.

Ingamells, C. O., 1970, Lithium metaborate flux in silicate analysis:
Analytical Chimica Acta, v. 52, p. 323-334.

Kuntz, M. A., 1977a, Extensional faulting and volcanism along the Arco rift
zone, eastern Snake River Plain, Idaho: Geological Society of America
Abstracts with Programs, v. 9, no. 6, p. 740-741.

_____1977b, Structural and volcanic characteristics of the eastern Snake River Plain, Idaho: National Aeronautics and Space Administration Technical Memorandum 78,436, p. 1-2.

_____1977c, Rift zones of the Snake River Plain, Idaho, as extensions of Basin-Range and older structures: Geological Society of America Abstracts with Programs, v. 9, no. 7, p. 1061-1062.

_____1978a, Stratigraphy of lava flows in drill holes at the proposed Safety Research Experiment facility (SAREF), Argonne National Laboratory-West, Idaho National Engineering Laboratory (INEL), Idaho: U.S. Geological Survey Open-File Report 78-665, 1 p.

_____1978b, Geology of the Arco-Big Southern Butte area, eastern Snake River Plain, and potential volcanic hazards to the Radioactive Waste Management Complex and other waste storage and reactor facilities at the Idaho National Engineering Laboratory, Idaho: U.S. Geological Survey Open-File Report 78-691, 70 p.

_____1978c, Geologic map of the Arco-Big Southern Butte area, Butte, Blaine, and Bingham Counties, Idaho: U.S. Geological Survey Open-File Report 78-302.

Kuntz, M. A., Scott, W. E., Skipp, Betty, Hait, M. H., Jr., Embree, G. F., Hoggan, R. D., and Williams, E. J., 1979, Geologic map of the Lava Ridge-Hells Half Acre area, eastern Snake River Plain, Idaho, U.S. Geological Survey Open-File Report 79-669.

Lanphere, M. A., and Dalrymple, G. B., 1976, Final compilation of K-Ar and Rb-Sr measurements on P-207, the U.S. Geological Survey, laboratory standard muscovite, _in_ Flanagan, F. J., Comp. and ed., Descriptions and analyses of eight new USGS rock standards: U.S. Geological Survey Professional Paper 840 p. 127-130.

LaPoint, P. J. I., 1977, Preliminary photo-geologic map of the eastern Snake
River Plain, Idaho: U.S. Geological Survey Miscellaneous Field Studies
Map MF-850.

Leeman, W. P., and Vitaliano, C. J., 1976, Petrology of the McKinney Basalt,
Snake River Plain, Idaho: Geological Society of America Bulletin, v. 87,
p. 1777-1792.

Mabey, D. R., 1976, Interpretation of a gravity profile across the western
Snake River Plain, Idaho: Geology, v. 4, p. 53-55.

_____1978, Regional gravity and magnetic anomalies in the eastern Snake River
Plain, Idaho: U.S. Geological Survey Journal of Research, v. 6, no. 5,
p. 553-562.

Mabey, D. R., Zietz, Isadore, Eaton, G. P., and Kleinkopf, M. D., 1978,
Regional magnetic patterns in part of the Cordillera in the Western
United States, in Smith, R. B., and Eaton, G. P., eds., Cenozoic
tectonics and regional geophysics of the Western Cordillera: Geological
Society of America Memoir 152, p. 93-106.

Macdonald, G. A., 1972, Volcanoes: Englewood Cliffs, New Jersey, Prentice-
Hall Inc., 510 p.

Malde, H. E., 1971, Geologic investigation of faulting near the National
Reactor Testing Station, Idaho, with a section on Microearthquake
studies, by A. M. Pitt and J. P. Eaton: U.S. Geological Survey Open-file
report, 167 p.

Malde, H. E., and Powers, H. A., 1962, Upper Cenozoic stratigraphy of the
western Snake River Plain, Idaho: Geological Society of America
Bulletin, v. 73, p. 1197-1220.

Mankinen, E. A., and Dalrymple, G. B., 1972, Electron microprobe evaluation of
terrestrial basalts for whole-rock K-Ar dating: Earth and Planetary
Science Letters, v. 17, p. 89-94.

Manson, Vincent, 1967, Geochemistry of basaltic rocks-- Major elements, _in_

Hess, H. H., and Poldervaart, Arie, eds., Basalts, the Poldervaart

treatise on rocks of basaltic composition, v. 1: New York, Interscience

Publishers, p. 215-270.

Prostka, H. J., and Embree, G. F., 1978, Geology and geothermal resources of

the Rexburg area, eastern Idaho: U.S. Geological Survey Open-File

Report 78-1009, 14 p.

Ruppel, E. T., 1964, Strike-slip faulting and broken basin-ranges in east-

central Idaho and adjacent Montana, _in_ Geological Survey Research 1969:

U.S. Geological Survey Professional Paper 501-C, p. C14-C18.

_____1978, Medicine Lodge thrust system, east-central Idaho and southwest

Montana, U.S. Geological Survey Professional Paper 1031, 23 p.

Schoen, R., 1974, Geology, Part III, _in_ Robertson, J. B., Schoen, R., and

Barraclough, J. T., The influence of liquid waste disposal on the

geochemistry of water at the National Reactor Testing Station, Idaho:

U.S. Geological Survey Open-File Report IDO-22053.

Scholten, Robert, 1957, Paleozoic evolution of the geosynclinal margin north

of the Snake River Plain, Idaho-Montana: Geological Society of America

Bulletin, v. 68, p. 151-170.

_____1973, Gravitational mechanisms in the northern Rocky Mountains of the

United States, _in_ DeJong, K. A., and Scholten, Robert, eds., Gravity and

tectonics: New York. John Wiley and Sons.

Shapiro, Leonard, 1975, Rapid analysis of silicate, carbonate, and phosphate

rocks, revised ed.: U.S. Geological Survey Bulletin 1401, 76 p.

Sherrill, N. D., and Dalrymple, G. B., in press, A computerized multichannel

data acquisition and control system for high-precision mass

spectrometry: U.S. Geological Survey Professional Paper.

Skipp, Betty, and Hait, M. H., Jr., 1977, Allochthons along the northeast

 margin of the Snake River Plain, Idaho: Wyoming Geological Association

 Guidebook, Twenty-ninth annual field conference, p. 499-515.

Smith, R. L., and Bailey, R. A., 1968, Resurgent cauldrons, in Coats, R. R.,

 Hay, R. L., and Anderson, eds., Studies in volcanology--A memoir in honor

 of Howel Williams: Geological Society of America Memoir 116, p. 613-662.

Spear, D. B., 1979, Evidence for mixing of rhyolite and basalt magmas at East

 Butte, eastern Snake River Plain, Idaho: Geological Society of America

 Abstracts with Programs, v. 11, no. 6, p. 303.

Stacey, J. S., Sherrill, N. D., Dalrymple, G. B., Lanphere, M. A., and

 Carpenter, N., 1978, A computerized five-collector mass spectrometer for

 precision argon analyses: U.S. Geological Survey Open-File

 Report 78-701, p. 411-413.

Stanley, W. D., Boehl, J. E., Bostick, F. X., and Smith, H. W., 1977,

 Geothermal significance of magnetotelluric soundings in the eastern Snake

 River Plain-Yellowstone region: Journal of Geophysical Research, v. 82,

 p. 2501-2514.

Steiger, R. N., and Jager, E., 1977, Subcommission on geochronology:

 Convention on the use of decay constants in geo- and cosmochronology:

 Earth and Planetary Science Letters, v. 36, p. 359-362.

Stewart, J. H., 1978, Basin-range structure in North America: A review, in

 Smith, R. B., and Eaton, G. P., eds., Cenozoic tectonics and regional

 geophysics of the Western Cordillera: Geological Society of America

 Memoir 152, P. 1-32.

Stone, G. T., 1967, Petrology of upper Cenozoic basalts of the Snake River

 Plain: Boulder, Colorado, University of Colorado Ph.D. thesis, 392 p.

Stout, M. Z., and Nicholls, J., 1977, Mineralogy and petrology of Quaternary

    lavas from the Snake River Plain, Idaho: Canadian Journal of Earth

    Sciences, v. 14, p. 2140-2156.

Thompson, R. N., 1975, Primary basalts and magma genesis, II, Snake River

    Plain, Idaho, U.S.A.: Contributions to Mineralogy and Petrology, v. 52,

    p. 213-232.

Tilley, C. E., and Thompson, R. N., 1970, Melting and crystallization

    relations of the Snake River basalts of southern Idaho: Earth and

    Planetary Science Letters, v. 8, p. 79-92.

Valastro, S., Jr., Davis, E. M., and Varela, A. G., 1972, University of Texas

    at Austin Radiocarbon dates IX: Radiocarbon, v. 14, p. 468-470.

Williams, Howel, 1932, The history and character of volcanic domes:

    University of California Publications in the Geological Sciences, v. 21,

    p. 51-146.

Yoder, H. S., and Tilley, C. E., 1962, Origin of Basaltic Magmas: An

    experimental study of natural and synthetic rock systems, Journal of

    Petrology, v. 3, p. 342-532.

Zohdy, A. A. R., and Stanley, W. D., 1973, Preliminary interpretation of

    electrical sounding curves obtained across the Snake River Plain from

    Blackfoot to Arco, Idaho: U.S. Geological Survey Open-file report.